

The big bang of an epidemic

Yazdan Babazadeh¹, Amin Safaeesirat², and Fakhteh Ghanbarnejad^{3,*}

¹Department of Applied Mathematics, University of Waterloo, Waterloo, ON N2L 3G1, Canada

²Department of Physics, Simon Fraser University, Burnaby, Canada

³Potsdam Institute for Climate Impact Research (PIK), Member of the Leibniz Association, P.O. Box 601203, Potsdam, 14412, Germany

*fakhteh.ghanbarnejad@gmail.com

May 8, 2024

Abstract

In this paper, we propose a mathematical framework that governs the evolution of epidemic dynamics, encompassing both intra-population dynamics and inter-population mobility within a metapopulation network. By linearizing this dynamical system, we can identify the spatial starting point(s), namely the source(s) (A) and the initiation time (B) of any epidemic, which we refer to as the "Big Bang" of the epidemic. Furthermore, we introduce a novel concept of effective distance to track disease spread within the network. Our analysis reveals that the contagion geometry can be represented as a line with a universal slope, independent of disease type (R0) or mobility network configuration. The mathematical derivations presented in this framework are corroborated by empirical data, including observations from the COVID-19 pandemic in Iran and the US, as well as the H1N1 outbreak worldwide. Within this framework, in order to detect the Big Bang of an epidemic we require two types of data: A) A snapshot of the active infected cases in each subpopulation during the linear phase. B) A coarse-grained representation of inter-population mobility. Also even with access to only type A data, we can still demonstrate the universal contagion geometric pattern. Additionally, we can estimate errors and assess the precision of the estimations. This comprehensive approach enhances our understanding of when and where epidemics began and how they spread, and equips us with valuable insights for developing effective public health policies and mitigating the impact of infectious diseases on populations worldwide.

1 Introduction

Throughout history, infectious disease outbreaks have significantly impacted human life all over the world [61, 48], causing many deaths [68]. For instance, the COVID-19 pandemic, originating from China [87], affected people of all countries [67, 84], mentally [71, 35, 80], financially [15], and beyond. Human mobility is a key factor in this regard [32, 22, 25, 17, 21, 5], accounting for the spatial spread of diseases, facilitating their propagation through the densely connected networks of global, national, local displacement [6, 82, 40]. The complex network of travel routes [20] provides numerous direct and indirect pathways for disease transmission at various scales, with air travel playing a crucial role in the rapid spread of viruses including SARS-CoV-2 [1, 27, 54, 4, 63] at the macroscopic level, given their potential to connect distant locations [11]. This underscores the importance of taking immediate non-pharmacological interventions [58], such as air travel restrictions [1, 8], to control disease spread. Understanding the underlying mechanisms of disease transmission at a coarse-grained level, where the mobility network can be considered as a meta-population network [10, 23], is essential for developing effective strategies to control pandemics and save lives. More specifically, answering questions like "Where is (are) the source (sources) of an epidemic?", "When did it begin?", which we refer to as the **Big Bang** of the epidemic, and "How does the outbreak spread through other sub-populations?" after the Big Bang, is of paramount importance.

In recent studies, a variety of mathematical models [70], ranging from stochastic models [65, 29], spatio-temporal spreading models [74, 66], reaction-diffusion [73], to agent-based [41, 64, 18, 33, 34] and network [11] models and meta-population models [18, 16, 83, 19, 28, 29, 13, 14, 12, 24, 38, 39, 42, 53, 55, 62, 9] have been developed to investigate various aspects of disease-spread phenomena. More specifically, **Effective Distance (ED)** can effectively address the issues stated above [36, 25, 54, 49, 88, 88, 2]. The effective distance between two sub-populations is defined based on the probability of travel through direct or indirect displacement paths between them. Considering the most probable path between two sub-populations, in 2007 Gautreau *et al* [36] and later in 2013 Brockmann and Helbing [25] proposed ansatz for calculating effective distance, and showed a relatively high correlation between ED and the first arrival time of a disease in simulations using the worldwide

air transportation network. The methodology was later improved by adding the effects of all possible paths [37], resulting in a substantial increase in the correlation between the first arrival time and ED. Also this approach has been validated with empirical data of the 2003 SARS and the 2009 H1N1 pandemics [25]. Other successful modifications on ED have also been reported [54, 49, 88]. For instance, Zhang *et al* introduced Country Distancing [88], which is similar to the equivalent resistance defined for parallel resistors in electrical circuits. The idea of ED was also successfully tested for the Covid-19 pandemic on the world air traffic data [2]. Furthermore, the ED method suggests a technique to identify the source of an epidemics by pinpointing the source that exhibits the highest correlation between arrival time and Effective Distance [25].

There are also many other methods developed to identify the source of an outbreak in a variety of networks such as a meta-population network or a network of individuals, and in different contexts like disease spreading [81, 56, 7, 85, 59, 72, 26], information spreading [60, 57, 3], food contamination [44, 43, 75], rumors [50, 78, 50, 76, 86, 51, 77], diffusion processes on networks [45, 46, 47, 79, 69, 30], etc. Typically, the aim of these studies is to identify the source of spread from a “snapshot”, for example number of infected ones, which is the state of the system after the start of the spread.

Despite the success of ED methods, there are some limitations. Some examples follow. First, their definitions often rely on intuition rather than being grounded in comprehensive mathematical models, which may hinder their clarity and interpretability, as well as impede a deep understanding of the contagious dynamics they aim to describe. Second, it is usually assumed that the disease originates from a specific location in the network (the source) and contaminates other nodes over time. However, this assumption is not necessarily true. For instance, on a country scale, the disease can reach different nodes (states or provinces) from outside the network during its spread, effectively acting as multi-sources within the country. Finally, the methods lack any correction of time to detect the beginning of the epidemic in data or any error analysis to check the validity of the spatial and temporal source estimations.

In this paper, we address these gaps by first developing a mathematical framework based on intra-population SIR model dynamics and inter-population mobility within a metapopulation network. We then derive expressions to identify the source or sources of any given epidemic, as well as its starting time, given the number of infected individuals and coarse-grained mobility data at a specific time. Additionally, we propose a novel definition for ED, which **universally** relates the overtaking time of nodes to their ED from the source of the epidemic. We validate our method using empirical data from the COVID-19 pandemic in Iran and the United States, as well as H1N1 worldwide.

2 Our Mathematical Framework

Here we aim to find the Big Bang of a given epidemic dynamics, and in particular, we want to understand how an outbreak spread after the Big Bang. In doing so, the first step is to propose our general mathematical framework which the spreading dynamics adhere to.

When studying the spread of infectious diseases at a given coarse-grained scale, the disease can be considered to spread through a meta population network. In this network, the number of infected and infectious individuals at time t and for subpopulation (node) i , $I_i(t)$, can be put into components of a vector we call $\vec{I}(t)$:

$$\vec{I}(t) = (I_1(t), I_2(t), \dots, I_n(t)). \quad (1)$$

In general, during epidemic dynamics, there is no specific pattern in the number of infected people across all nodes. However, typically, the number initially increases to reach a peak, followed by a subsequent decline, see Fig. 1(A). In our following framework, our primary objective is to demonstrate the evolution of $\vec{I}(t)$ and subsequently discern a straightforward geometric pattern that illustrates the progression of the outbreak within nodes of the metapopulation network. Therefore we show that vector $\vec{I}(t)$ evolves in time as follows, see Fig. 1(B) and the Supplementary Material (S.M.), Section 6 for more details:

$$\vec{I}(t) = e^{\hat{B}pt} \vec{I}(0). \quad (2)$$

The above equation is the solution of the following equation, assuming $S_i \approx N_i$ for the early stages of the dynamic, see S.M. 6.4 for more details:

$$\frac{dI_i}{dt} = [\beta_i S_i I_i - \gamma_i I_i] + [p \sum_j P_{ji} I_j - p I_i]. \quad (3)$$

While this equation represents the dynamic of vector $\vec{I}(t)$ and has two parts:

1. spreading within the population, namely **intra population** (First Bracket).
2. spreading between nodes, namely **inter population** (Second Bracket).

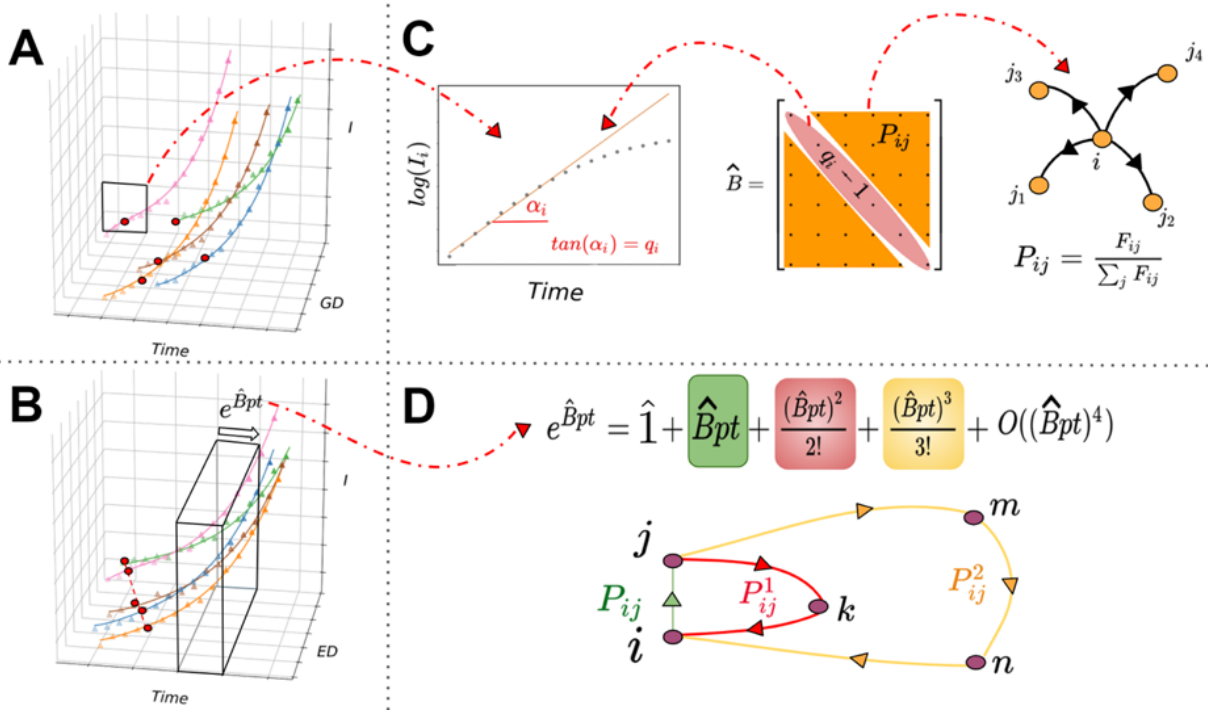


Figure 1: **(A)** The number of infected people in different nodes ($\vec{I}(t), 1$) in a network versus time. The third dimension represents the geographical distance from the source in this specific network and it does not show any pattern. **(B)** The same number of infected people in different nodes in a network versus time; but this time they are plotted based on their effective distances from the source. This time a linear relation between the overtaking times and **Effective Distances** can be seen. The evolution of the number of infected people is given by the operator, $e^{\hat{B}pt}$, see Eq. 2. **(C) Center:** The matrix \hat{B} is defined based on the transition probability (see S.M. 6.2) and the slope of the linear part of the SIR dynamics (see S.M. 6.4). **left:** $\log I_i$ vs time is illustrated. q_i is the slope of the linear part. The behavior of $\log(I_i)$ in the early stage of the dynamic is linear and the slope of this line is q_i . **Right:** the transition probability is made from the flow between node i and j . **(D)** When $e^{\hat{B}pt}$ is expanded several terms are generated, each containing a power of matrix P . Different terms generate the probability of intermediary transitions. For example, the κ_{th} term of the expansion corresponds to a path containing $\kappa - 1$ intermediary node.

For the first part of the equation, we use a simple Susceptible-Infected-Recovered model (SIR) with a homogeneous mean field approximation (HMFA). Moreover, in the second bracket, we connect all nodes, i.e. each population via a meta-population network. A detailed explanation of how the intra-population term in Equation 3 is derived can be found in S.M., Sections 6.2 and 6.3.

In Eq.2, matrix \hat{B} keeps all of the information regarding the properties of the dynamics (Fig. 1(C), center). The diagonal components (q_i) represent the properties of internal growth of the disease (Intra Population Dynamics). The population of infected people in each node shows exponential behavior at early stages. So, in the plot of $\log(I)$ vs time, there is a linear pattern for each node at the beginning of the outbreak called "linear phase". In this study, we specifically focus on this part of the dynamics. As it can be seen in Fig.1(C), left, the slope of this line for node i is q_i , which sits into the i_{th} diagonal component of matrix \hat{B} (Fig. 1(C), center), see more details in S.M. 6.5.

Other components of matrix \hat{B} are called P_{ij} , which represent the probability of traveling from node i to j . For calculating the value of P_{ij} we use the flow matrix, F_{ij} , which keeps the number of people who travel from node i to j in a specific period. (Fig. 1(C), Right). Further details about probability and flow matrices are available in the S.M. 6.2.

Now we can expand the solution (Eq. 2) and write it down as:

$$\vec{I}(t) = (\hat{1} + \hat{B}pt + \frac{(\hat{B}pt)^2}{2} + \dots)\vec{I}(0) \quad (4)$$

This expansion contains different powers of matrix \hat{B} . Since \hat{B} has P_{ij} on its non-diagonal components, different powers of \hat{B} generate different powers of matrix P . As matrix P describes the probability of transition directly from node i to j , higher powers of P describe the probability of indirect transition from node i to

j through a specific number of intermediary nodes in between. This is a new finding we call **Intermediate Probability**. As can be seen in Fig.1(D), the k_{th} component of the expansion holds the intermediate probability of using $\kappa - 1$ intermediary nodes (S.M. 6.6).

The expanded solution can get simpler even further by focusing on the early stage of the dynamic, i.e. the linear phase, and because it takes more time to transit by indirect paths via intermediate nodes. This means that in the early stages of the dynamics, as we go further into the expansion, terms become smaller. Therefore, we can simplify the dynamic by cutting the expansion up to a certain term, keeping only the first terms. This defines the time scales for our model framework. We need to be in a time range in which the assumption of linear evolution for SIR and expansion's cut work together, or $\tau = \min\{\frac{1}{\beta-\gamma}, \frac{1}{p}\}$, which constrains the time scale.

As explained, we aim to focus on the very beginning of the spread process, when everything just started and almost no one was infected, and study the expansion of the number of infected individuals in a specific order from the start, like the idea of the **Big Bang** in cosmology. In the following section, we will introduce several algorithms to solve the challenges and find the starting time and place as well as the hidden spread mechanism of the disease.

3 Algorithms and Results

In this section, using our mathematical framework, we introduce algorithms that reveal **where** and **when** the outbreak began and **how** it spread further using the snapshots of the disease and the flow matrix. In the first algorithm, we detect the potential sources of the disease. In the second one, we estimate the starting time of the spread, then we introduce an algorithm to illustrate a geometric pattern for the spread of the disease. There are different sources of error in the estimations such as approximating the outbreak with SIR model, inaccurate measurement of the number of infected people, and the flow matrix, which is challenging to take into account. Therefore, we only report the theoretical error caused by the cut-off in the expansion of $\exp \hat{B}pt$ operator, see details in S.M. Sections 7.3 and 7.5. And the role of estimating epidemiological parameters in error analysis is discussed in the supplementary text (S.M., Section 10). Given that these algorithms rely on empirical data as input, to distinguish empirical data from theoretical variables, we denote empirical data using the subscript or superscript **e**. For instance, $\vec{I}(t)$ is a vector containing the number of infected people in our mathematical framework, and $\vec{I}^e(t)$ is the same vector but contains the empirical data of infected people coming from official reports and announcements, see S.M. Sec. 9.

3.1 Where did it start?

Here, we aim to find the potential sources, **where** the dynamic began, having $\vec{I}^e(t)$ as empirical data and (Eq.2) as theoretical formalism. We first develop the theoretical basis of the algorithm and then discuss how to apply it to COVID-19 data of Iran and the USA.

In a network with n nodes, there is a n -dimensional vector space whose i -th basis represents the node i . We define the basis \vec{i} as

$$\vec{i} = (0, 0, \dots, 1, \dots, 0), \quad (5)$$

in which its i -th component is 1 and others are zeros. Now we can expand vector $\vec{I}(t)$ in this space using these bases. The value of the component of this vector on each basis indicates the contribution of that basis to the spread of the disease. As can be seen in Eq. 2, the vector $\vec{I}(t)$ evolves in time and we have to evolve the bases in time as well, to rewind the dynamic to the origin of the time (see S.M. 7.1). Therefore, we redefine the bases as follows:

$$\vec{i}' = e^{\hat{B}pt} \vec{i}. \quad (6)$$

Now, we define the "weight of a node" as:

$$W_i = \frac{\vec{i}' \cdot \vec{I}(t)}{\sum_{\vec{j}} \vec{j}' \cdot \vec{I}(t)}, \quad (7)$$

in which W_i is a number between 0 and 1 that shows the impact and contribution of the node i on the spreading and evolution of the disease at any time within the linear range of the dynamic. If t is measured exactly from the **origin of time** of the disease, then W_i represents the **spatial source of the disease**, which can be a single or multiple source. For example, for a given network if $W_i = 1$, it means that node i was the only source of the network. For empirical data we use the vector $\vec{I}^e(t_e)$ in Eq. 7, instead of vector $\vec{I}(t)$. t_e is time, measured from the officially reported temporal origin of the disease. Therefore

$$W_i^e = \frac{\vec{i}' \cdot \vec{I}^e(t_e)}{\sum_{\vec{j}} \vec{j}' \cdot \vec{I}^e(t_e)}. \quad (8)$$

It is important to note that W_i^e calculation is independent of the structure of the network as there is no constraint (such as topology of the network) on the flow matrix used in the calculation.

In figure 2, we implement this method for the empirical COVID-19 data of Iran and the US (Panel A and A') and illustrate the results. Also the mobility probability matrix are plotted respectively in panels B and B'. In the case of Iran (Panel C and D), we observe that the values of weights differ by implementing different snapshots. In the first scenario, Qom has the highest weight value, but when considering data from later days, Tehran (the capital province of Iran) surpasses it. Since the largest international airport in Iran (Imam Khomeini) is located between Qom and Tehran provinces, and other important nodes like Gilan and Mazandaran (which also have high values of W) are geographically close to this airport, we can conclude that it is more probable that the very first seed of the disease came from this airport to the country and Tehran and Qom are the most probable sources of the disease, which is consistent with official reports. For the case of the US, (C' and D') Washington state has the highest value of weight in the first plot, but over time, based on the values of W , and error bars, other states like Michigan, California, and New York could also be considered important nodes. So, based on this figure, our model predicts that the states of Washington, Michigan, and New York were the most probable sources of the pandemic in The US.

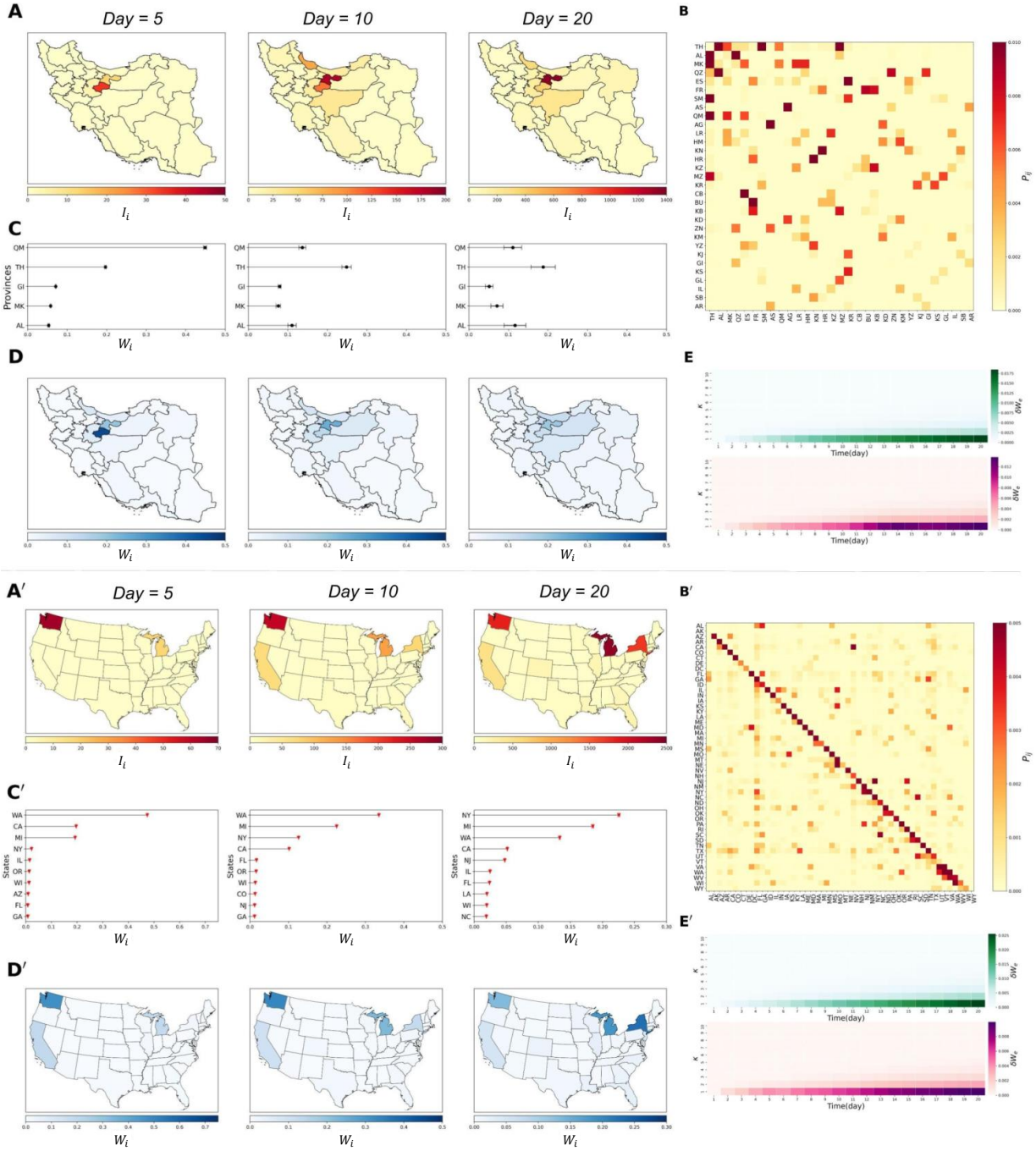


Figure 2: **Where did it start?** For better visibility of details, please zoom in. **A&A')** In these color maps, the number of COVID-19 infected individuals ($\bar{I}^e(t_e)$) is depicted across various provinces/states of Iran/the United States, captured at different snapshots ($t_e = 5, 10, 20$ days). The time origin of these snapshots is the official start day of the pandemic in these two countries. **B&B')** The color map demonstration of the mobility probability matrix, used to calculate the values of W_i^e for Iran/United States. Please refer to the S. M. Section 9 for more details regarding the data. **C & C')** W_i^e (Eq.8), is illustrated for provinces/states of Iran/United States. The black/red points represent the estimated value of W_i^e for each node, and the black/red bars illustrate the value of errors, δW_i^e . We used the first three terms of the Taylor expansion to calculate weights and errors. Please refer to S.M. 7.1 for more details. **D&D')** The W_i^e shown in panels C and C' are visualized on geographical maps. **E&E')** These plots illustrate the reliability of different κ values for the cut-off error. The magnitude of $|\delta \vec{W}^e|$ is depicted in the top color map for the empirical data and in the bottom color map for the simulation results for the networks of Iran and the United States. The vertical axis represents κ , while the horizontal axis represents time. Here attention should be given to the values of $\kappa = 3$ and time (5, 10, 20) used in panels C and C', as they are indicated in both color maps. We considered $R_0 = 3$ (Basic Reproduction Number) and $\frac{1}{\gamma} = 14(\text{days})$ for all nodes. Please refer to S.M. 10 for sensitivity analysis.

The reasons for these fluctuations can be the uncertainty in empirical data (error in testing, organization error, and other sources of errors), deviation from the assumption of our model (see discussion section), and errors in calibration (q_i and p).

To calculate the error of the Eq. 7 and Eq. 8 we consider the value of **cut-off error** since only the first terms of the Taylor expansion of e^{Bpt} is used in the calculations. If W_i^e is calculated using the first κ terms of the e^{Bpt} expansion, the error of W_i^e can be calculated using $\kappa+1$ term as

$$\delta W_i^e = \frac{\left(\frac{t^{\kappa+1} B^{\kappa+1}}{\kappa!} \vec{i}'\right) \cdot \vec{I}^e(t_e)}{\sum_{\vec{i}'} \vec{i}' \cdot \vec{I}^e(t_e)}. \quad (9)$$

The value of error depends both on κ and the value of t_e . By increasing κ or decreasing t_e , we expect to get a smaller value of error. To get a better idea from the value of cut-off error in a whole network, we define the **error of cut-off vector** as:

$$|\delta \vec{W}^e| = \frac{\sqrt{\sum_i (\delta W_i^e)^2}}{n}, \quad (10)$$

which is shown versus κ and t_e for Iran (panel E) and the US (panel E').

3.2 When did it start?

In this section, our goal is to estimate the temporal origin of the outbreak. As we already mentioned, the real origin of time may differ from the one that is officially reported. To find the temporal origin we compare the estimated ($\vec{I}(t)$) and reported ($\vec{I}^e(t_e)$) number of infected people at the time t and t_e , respectively. We find the temporal origin so that it minimizes the mean squared error (MSE) between $\vec{I}(t)$ and $\vec{I}^e(t_e)$,

$$\Delta_i(t) = \frac{\sum_{j=1}^n (I_j(t) - I_j^e(t_e))^2}{n}. \quad (11)$$

To estimate the number of infected people, $\vec{I}(t)$, we assume the source is the node i found by the **Where** algorithm, Sec. 3.1. Eq. 11 has a unique minimum at time t_i^* (see S.M. 7.2 and (Fig. 3)) :

$$t_i^* = \frac{1 - \eta(i_0 - I_i^e(t_e)) + p \sum_j (P_{ij} I_j^e(t_e))}{\eta^2 + p^2 \sum_j P_{ij}^2}, \quad (12)$$

in which $\eta = (\beta_i N_i - \gamma_i - p)$, and i_0 is the initial number of the infected people in the source and at t_i^* (the estimate of the model for the temporal origin of the outbreak). For the error, we consider the cut-off error by adding the third term of the Taylor expansion as the error-making term to our calculation which shows how the predictions degrade (S.M. 7.3).

Fig. 3 demonstrates the result of our algorithm applied to the empirical data of Iran and the US. In panel **A** and **C**, Δ (Eq.11) is shown versus time for Iran and the US, respectively. A minimum exists in both cases, as we showed in Eq.12. By adding the third term of the Taylor expansion (Eq.4) to the calculation, the corrected MSE (specified with different colors) shifts to a new curve and the minimum moves a bit (around two days for Iran and less than a day for the US). To understand the accuracy of the algorithm, we illustrate t_i^* versus t_e for Iran (panel **B**) and the US (panel **D**) using snapshots from various days. A linear behavior can be observed up to a certain point in both cases, which indicates the linear range of the dynamics. It is worth noting again that t_i^* describes the starting time of the disease from the epidemiological point of view, while t_e refers to the starting time the official reports claim. So, a difference between these two origins of time is expected. By utilizing these specific snapshots, the onset of the COVID-19 pandemic is estimated to be 8 February 2020 for Iran and 12 February 2020 for the US, marking the commencement of the widespread outbreak in Iran and the US.

3.3 How does it spread? The universal pattern of any outbreaks

In previous sections, we estimated the origin of the disease, trying to answer when and where it began. In this section, we aim to illustrate the simple geometric patterns behind the dynamics.

For the first step, let us define the **overtaking time** in our mathematical formalism. This is the time when enough number of infected passengers arrive in a susceptible node so that we can consider this node as infected. We assume that it happens when the intra-population spreading in this node (the first bracket in Eq. 3) becomes greater than the inter-population spreading (the second bracket in Eq. 3), which means

$$(N_j \beta_j - \gamma_j) I_j = p \left(\sum_k P_{kj} I_k - I_j \right). \quad (13)$$

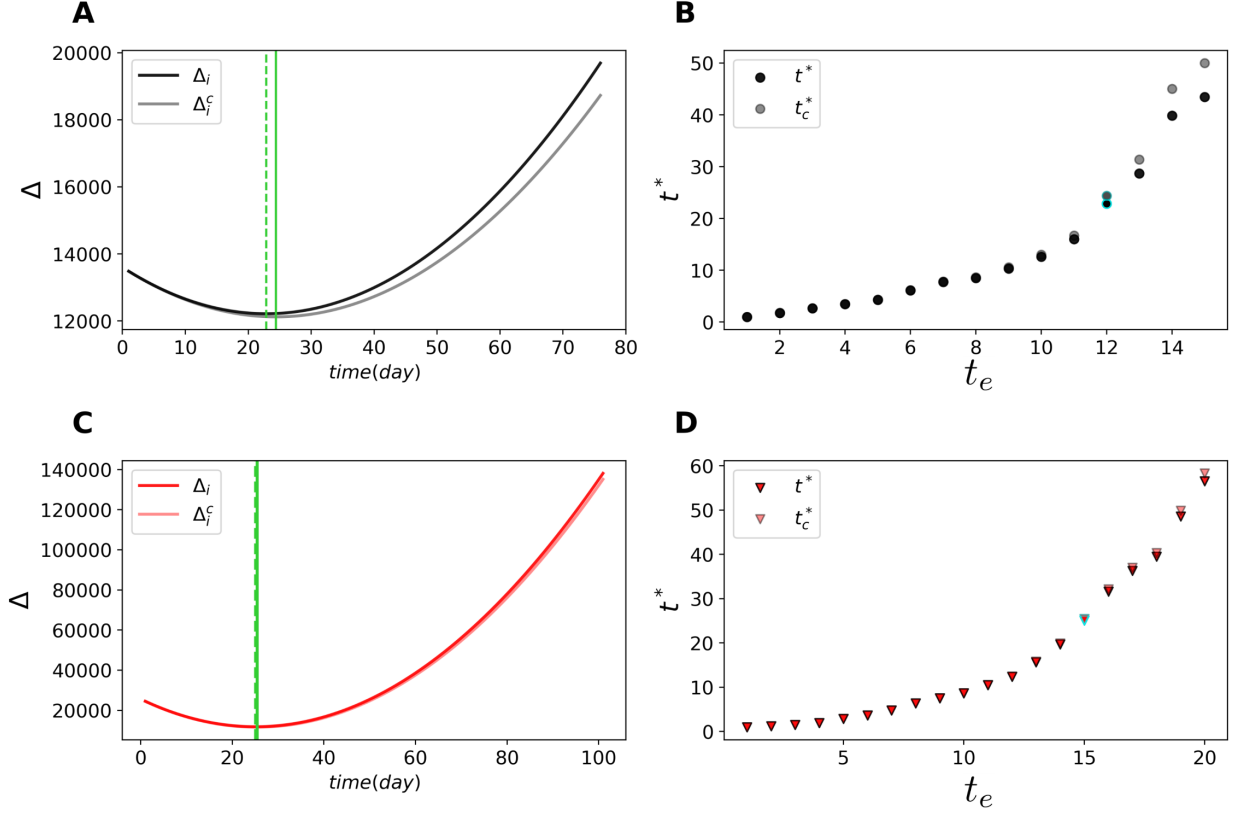


Figure 3: **When did it start?** **A)** The value of MSE (Eq.11) is illustrated versus time (the black curve) for Qom province using a snapshot for the 12th day of the COVID-19 pandemic in **Iran**. As shown, it has a minimum at (t_i^*) (Eq.12). When the third term of the expansion is added to the calculation, Δ_i transforms to the gray curve (Δ_i^c), with the minimum shifted approximately two days. **B)** The estimated origin of time (t_i^*) versus the date of the snapshot (t_e) for Iran, considering Qom as the origin node. The points highlighted in green show the used snapshot in panel **A**. **C)** The value of MSE (Eq.11) is illustrated versus time (the red curve) for the Washington state using a snapshot for the 15th day of the COVID-19 pandemic in **the United States**. It has a minimum at (t_i^*) (Eq.12). When the third term of the expansion is added to the calculation, Δ_i transforms to the pink curve (Δ_i^c), which approximately lies on the red curve. **D)** The estimated origin of time (t_i^*) versus the date of the snapshot (t_e) for the US, considering Washington as the origin node. The points highlighted in green show the used snapshot in panel **C**. Please refer to the S. M. Section 9 for more details regarding the data.

Using the above condition and the dynamic of our model given by Eq. 4 , one can show that the overtaking time is (see S.M. Sections 7.4 and 7.5 for more details)

$$t_O^j = \frac{1}{p(2 + q_i - q_j) - \frac{P_{ij}^1}{P_{ij}}}, \quad (14)$$

in which the overtaking time, t_O^j , has been calculated for the node j, given the single source, node i, in the network.

To detect a simple **geometric pattern** of the spread dynamic, as shown in Fig. 1.b, we define an **Effective Distance** between a non-origin node j and the single origin node i so that there is a **linear relation** between overtaking time (Eq. 14). Therefore, our effective distance is defined as

$$D_{ij} = \frac{1}{(2 + q_i - q_j) - \frac{P_{ij}^1}{P_{ij}}}, \quad (15)$$

where

$$D_{ij} = pt_O^j. \quad (16)$$

Our innovative approach to defining effective distance distinguishes itself from previous methods [36, 37, 25]. While maintaining a similar geometric pattern of spread, our method uniquely utilizes overtaking time rather than arrival time. Remarkably, we reveal a **universal** behavior, characterized by a consistent **slope of one** when

plotting D_{ij} against pt_O^j , regardless of network or disease characteristics. In the above equation, p represents the inter-population speed of the disease spread among the nodes in a network.

Our proposed effective distance becomes simpler for some special cases. For example, if all nodes have the same value of q , the effective distance simplifies as

$$D_{ij} = \frac{1}{2 - \frac{P_{ij}^1}{P_{ij}}}, \quad (17)$$

which is independent of the disease properties and only depends on the the travel flow. The defined effective distance only includes those nodes that satisfy $\frac{P_{ij}^1}{P_{ij}} < 2$ as effective distance and the overtaking times should be positive for the non-origin nodes.

Fig. 4 shows the result of the effective distance analysis in two panels. In both panels, the spreading of the disease has been simulated with the SIR model for meta-population networks using the empirical mobility data of Iran (panel A) and the empirical mobility network of the United States (panel B). In each panel, the simulation has been repeated twice (Green and Gray in the left panel, Blue and Red in the right panel), each time with a different source node. The **Where** algorithm is used in the specific choice of the source nodes. As shown, there is a linear relation between the defined effective distance and pt , with the universal slope of one. Changing the source node does not change the linear relation and the value of the slope.

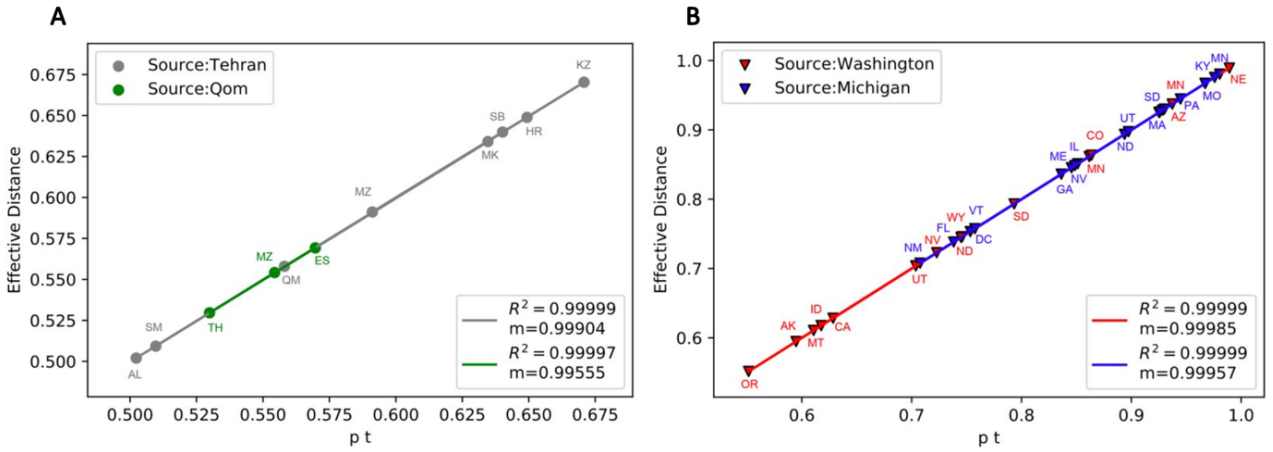


Figure 4: **Effective distance vs overtaking time (simulation result)**: The effective distances are illustrated versus pt_O^j (Eq.15) for the empirical mobility data of Iran (Panel A) and the United States (Panel B). Each panel represents two scenarios: we put the initial seed of the disease on a different node in each scenario. These two nodes are selected from the nodes with the higher chance of being the original COVID-19 source in Iran and the US based on the **Where** algorithm results. In each scenario, we simulated the spread of the disease in the network assuming $R_0 = 3$ (Basic Reproduction Number) and $\frac{1}{\gamma} = 14$ days for all nodes. In panel A, Gray/Green nodes represent the results of the simulation for Tehran/Qom, respectively as the source nodes. Also, the gray and Green lines are the best-fitted lines to the data, with their slope and regression shown in the legend. In Panel B, Red/Blue nodes represent the simulation results for Washington/Michigan as source nodes, with the Red and Blue lines showing the best-fitted lines to the data. Please refer to the S. M. Section 9 for more details regarding the mobility data.

Implementing effective distance analysis with empirical data can pose several challenges. Some of these are outlined below. First, what is reported as the arrival time in official data is not necessarily the same as what we defined as overtaking time in Eq. 14, even though they are close. Second, measuring the exact value of the mobility probability matrix is difficult, especially due to the intervention policy in each region at the beginning. Finally, the initial number of infected people (i_0) is not necessarily known.

It is possible to overcome the challenges stated above by estimating the effective distance of the node j from the source using the number of infected people in that node ($I_j^e(t_e)$). Using the mathematical framework, one can show that $I_j^e(t_e)$ can be estimated by a parabola (see S.M. Eq. 86) in the short enough period of time after the arrival of the disease to the node. Assuming the overtaking time occurs no longer after the arrival time, we estimate the effective distance of the node j from the source only by the found parameters from the fit (S.M. 7.6)

Fig. 5 shows the estimated effective distance and overtaking time for the empirical data of the COVID-19 pandemic in Iran (panel A), the US (panel B), and the H1N1 pandemic in 2009 in the meta-population of the world. As shown, there is a linear relation between effective distance and overtaking time in all instances, with

the universal slope close to 1. This result demonstrates that the linear relation with a slope of one remains independent of both the disease type and the size and structure of the meta-population network in which the disease spreads.

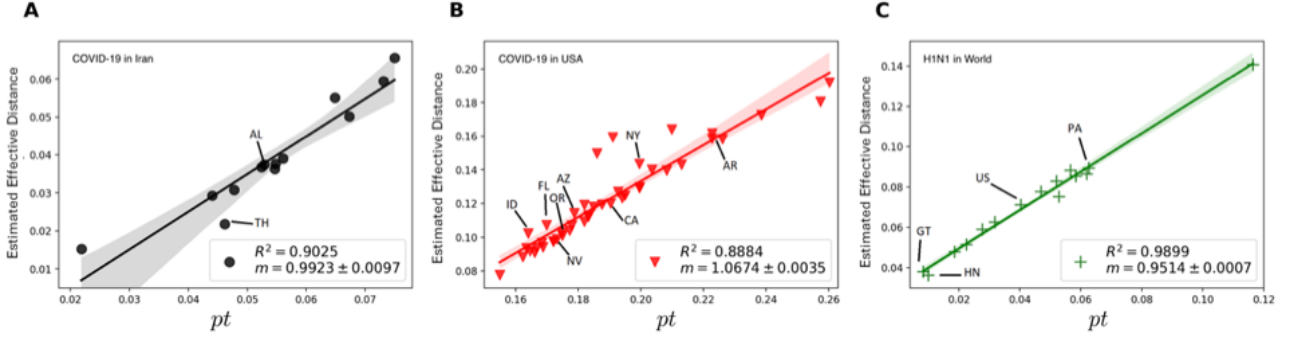


Figure 5: **Estimated effective distance vs overtaking time (empirical data result)**: The estimated effective distance (S.M. 7.6) versus the scaled overtaking time (pt) is illustrated for **A**) the Covid-19 pandemic in Iran, **B**) the Covid-19 pandemic in the United States, and **C**) H1N1 pandemic in the world (2009), based on the empirical data ($\vec{I}^e(t_e)$) of the pandemics. Please refer to the S. M. Section 9 for more details regarding the data.

4 Concluding Remarks

In summary, we introduced a mathematical framework based on the SIR model for meta-population networks, incorporating inter-population mobility. We derived a compact equation (Eq. 2) that represents the time evolution of the number of infected individuals using the mathematical operator $e^{\hat{B}pt}$. We showed how different terms in the Taylor expansion of the operator represent possible transmission paths with different number of intermediary nodes. Based on this general mathematical framework and the provided data, we were able to determine where and when the outbreak began, as well as how it spread within the meta-network.

Firstly, we derived a measure indicating the contribution of each node to disease spread, whether in single-source or multi-source pandemics. Our analysis of COVID-19 revealed that Qom, Tehran, Gilan, and Mazandaran carry the greatest weight in Iran, indicating these provinces as probable sources of the pandemic. This observation aligns with the proximity of these provinces to Imam Khomeini International Airport and the relatively high volume of travel to these areas. Likewise, Washington, Michigan, New York, and California were identified as likely sources of the pandemic in the US.

Secondly, we derived an expression to find the temporal origin of a pandemic. Thus, we estimated the beginning date of the COVID-19 pandemic in Iran and the US is Feb. 8, 2020, and Feb. 12, 2020, respectively. These dates precede the officially announced start dates in both countries, suggesting that the pandemic may have begun earlier than previously thought.

Thirdly, we introduced a novel definition for Effective Distance and demonstrated that the effective distance of a node from the source exhibits a linear relationship with the scaled overtaking time (pt), characterized by a universal slope of one. Importantly, this relationship remains independent of the epidemiological parameters of the disease and characteristics of the meta-population network, such as the number of passengers and network structure. This assertion is supported by our simulation results for Iran and the US. Finally, we showed how the effective distance can be estimated only with the data of the number of infected ones in the network. We applied this method to the data from the COVID-19 pandemic in Iran and the US, as well as the 2009 H1N1 pandemic. Our analysis confirmed the existence of a linear relationship with the universal slope of one.

Combining all reported observations, our analysis underscores the following practical implications: Given that the speed of disease propagation in the network is directly proportional to travel probability, p , this emphasizes the crucial role of implementing travel restrictions during the early stages of a pandemic. Additionally, our findings highlight the importance of predicting more accurately when and how diseases reach the next node. This insight provides policymakers with a better understanding of the optimal strategies for implementing lockdowns or travel restrictions, thereby effectively mitigating the spread of infectious diseases.

Our work presents several theoretical implications and prospects for the research community. Firstly, unlike similar studies [36, 37, 25], our definition of effective distance in this paper is directly derived from the mathematical model that describes the phenomenon, rather than relying solely on intuition or data analysis. Additionally, our analysis reveals that effective distance exhibits a universal geometric pattern, contributing to a

deeper understanding of epidemic dynamics across different contexts. Secondly, our study addresses fundamental questions such as where and when pandemics begin within a coherent mathematical framework, shedding light on essential aspects of disease spread. However, our method has limitations stemming from the simplifying assumptions we made. Firstly, we utilized the SIR model for meta-population networks, which can be extended by incorporating more complex epidemiological models, see S.M. Section 8 as an example. Secondly, we treated certain parameters as fixed, which may not always hold true. For instance, we assumed that the number of susceptible individuals remains constant and equal to the node's population at the early stage of the dynamic. Additionally, we supposed that γ is constant across nodes and that the flow matrix remains fixed over time. While these assumptions are reasonable in many cases, they may not accurately reflect reality in all scenarios. Furthermore, as demonstrated, systematic errors can arise from ignoring higher-order terms of the Taylor expansion (Eq. 4). Therefore, our algorithms and results can be enhanced by avoiding mathematical simplifications and improving data quality. Each of these aspects warrants further investigation in future studies.

5 Acknowledgement

The authors would like to acknowledge Yamir Moreno for his valuable comments and express gratitude to Hossein Afshin for providing us with Iran's passenger flow data.

References

- [1] Aniruddha Adiga, Srinivasan Venkatramanan, James Schlitt, Akhil Peddireddy, Allan Dickerman, Andrei Bura, Andrew Warren, Brian D Klahn, Chunhong Mao, Dawen Xie, et al. Evaluating the impact of international airline suspensions on the early global spread of covid-19. *medRxiv*, 2020.
- [2] Alberto Aleta and Yamir Moreno. Evaluation of the potential incidence of covid-19 and effectiveness of containment measures in spain: a data-driven approach. *BMC medicine*, 18:1–12, 2020.
- [3] Fabrizio Altarelli, Alfredo Braunstein, Luca Dall’Asta, Alejandro Lage-Castellanos, and Riccardo Zecchina. Bayesian inference of epidemics on networks via belief propagation. *Physical review letters*, 112(11):118701, 2014.
- [4] Roy M Anderson, Hans Heesterbeek, Don Klinkenberg, and T Déirdre Hollingsworth. How will country-based mitigation measures influence the course of the covid-19 epidemic? *The lancet*, 395(10228):931–934, 2020.
- [5] Roy M Anderson and RM May. Infectious diseases of humans. *Dynamics and Control*. Oxford, England: Oxford University Press, 1991.
- [6] Pol Antràs, Stephen J Redding, and Esteban Rossi-Hansberg. Globalization and pandemics. Technical report, National Bureau of Economic Research, 2020.
- [7] Nino Antulov-Fantulin, Alen Lančić, Tomislav Šmuc, Hrvoje Štefančić, and Mile Šikić. Identification of patient zero in static and temporal networks: Robustness and limitations. *Physical review letters*, 114(24):248701, 2015.
- [8] Alex Arenas, Wesley Cota, Jesús Gómez-Gardeñes, Sergio Gómez, Clara Granell, Joan T Matamalas, David Soriano-Paños, and Benjamin Steinegger. Modeling the spatiotemporal epidemic spreading of covid-19 and the impact of mobility and social distancing interventions. *Physical Review X*, 10(4):041055, 2020.
- [9] J Arino, S Portet, N Bajeux, and AS Ciupeanu. Investigation of global and local covid-19 importation risks. *Report to the Public Health Risk Science division of the Public Health Agency of Canada*, 2020.
- [10] Julien Arino. Spatio-temporal spread of infectious pathogens of humans. *Infectious Disease Modelling*, 2(2):218–228, 2017.
- [11] Julien Arino. Describing, modelling and forecasting the spatial and temporal spread of covid-19: A short review. In *Mathematics of Public Health: Proceedings of the Seminar on the Mathematical Modelling of COVID-19*, pages 25–51. Springer, 2021.
- [12] Julien Arino, Jonathan R Davis, David Hartley, Richard Jordan, Joy M Miller, and P Van Den Driessche. A multi-species epidemic model with spatial dynamics. *Mathematical Medicine and Biology*, 22(2):129–142, 2005.
- [13] Julien Arino and Stéphanie Portet. Epidemiological implications of mobility between a large urban centre and smaller satellite cities. *Journal of mathematical biology*, 71(5):1243–1265, 2015.
- [14] Julien Arino and P Van den Driessche. A multi-city epidemic model. *Mathematical Population Studies*, 10(3):175–193, 2003.
- [15] Badar Nadeem Ashraf. Economic impact of government interventions during the covid-19 pandemic: International evidence from financial markets. *Journal of behavioral and experimental finance*, 27:100371, 2020.
- [16] Paolo Bajardi, Chiara Poletto, Jose J Ramasco, Michele Tizzoni, Vittoria Colizza, and Alessandro Vespignani. Human mobility networks, travel restrictions, and the global spread of 2009 h1n1 pandemic. *PloS one*, 6(1):e16591, 2011.
- [17] Duygu Balcan, Vittoria Colizza, Bruno Gonçalves, Hao Hu, José J Ramasco, and Alessandro Vespignani. Multiscale mobility networks and the spatial spreading of infectious diseases. *Proceedings of the National Academy of Sciences*, 106(51):21484–21489, 2009.
- [18] Duygu Balcan, Hao Hu, Bruno Goncalves, Paolo Bajardi, Chiara Poletto, Jose J Ramasco, Daniela Paolotti, Nicola Perra, Michele Tizzoni, Wouter Van den Broeck, et al. Seasonal transmission potential and activity peaks of the new influenza a (h1n1): a monte carlo likelihood analysis based on human mobility. *BMC medicine*, 7(1):1–12, 2009.

- [19] Duygu Balcan and Alessandro Vespignani. Invasion threshold in structured populations with recurrent mobility patterns. *Journal of theoretical biology*, 293:87–100, 2012.
- [20] Albert-László Barabási, Réka Albert, and Hawoong Jeong. Mean-field theory for scale-free random networks. *Physica A: Statistical Mechanics and its Applications*, 272(1-2):173–187, 1999.
- [21] Hugo Barbosa, Marc Barthelemy, Gourab Ghoshal, Charlotte R James, Maxime Lenormand, Thomas Louail, Ronaldo Menezes, José J Ramasco, Filippo Simini, and Marcello Tomasini. Human mobility: Models and applications. *Physics Reports*, 734:1–74, 2018.
- [22] Vitaly Belik, Theo Geisel, and Dirk Brockmann. Natural human mobility patterns and spatial spread of infectious diseases. *Physical Review X*, 1(1):011001, 2011.
- [23] Derdei Bichara and Abderrahman Iggidr. Multi-patch and multi-group epidemic models: a new framework. *Journal of mathematical biology*, 77(1):107–134, 2018.
- [24] Wolfgang Bock and Yashika Jayathunga. Optimal control of a multi-patch dengue model under the influence of wolbachia bacterium. *Mathematical biosciences*, 315:108219, 2019.
- [25] Dirk Brockmann and Dirk Helbing. The hidden geometry of complex, network-driven contagion phenomena. *science*, 342(6164):1337–1342, 2013.
- [26] Jaeyoung Choi. Epidemic source detection over dynamic networks. *Electronics*, 9(6):1018, 2020.
- [27] Vittoria Colizza, Alain Barrat, Marc Barthélemy, and Alessandro Vespignani. The role of the airline transportation network in the prediction and predictability of global epidemics. *Proceedings of the National Academy of Sciences*, 103(7):2015–2020, 2006.
- [28] Vittoria Colizza and Alessandro Vespignani. Invasion threshold in heterogeneous metapopulation networks. *Physical review letters*, 99(14):148701, 2007.
- [29] Vittoria Colizza and Alessandro Vespignani. Epidemic modeling in metapopulation systems with heterogeneous coupling pattern: Theory and simulations. *Journal of theoretical biology*, 251(3):450–467, 2008.
- [30] Cesar Henrique Comin and Luciano da Fontoura Costa. Identifying the starting point of a spreading process in complex networks. *Physical Review E*, 84(5):056105, 2011.
- [31] Artis Curiskis and et al. The COVID Tracking Project at The Atlantic. <https://covidtracking.com/about-data>, March 2021.
- [32] Benjamin D Dalziel, Babak Pourbohloul, and Stephen P Ellner. Human mobility patterns predict divergent epidemic dynamics among cities. *Proceedings of the Royal Society B: Biological Sciences*, 280(1766):20130763, 2013.
- [33] Stephen Eubank, Hasan Guclu, VS Anil Kumar, Madhav V Marathe, Aravind Srinivasan, Zoltan Toroczkai, and Nan Wang. Modelling disease outbreaks in realistic urban social networks. *Nature*, 429(6988):180–184, 2004.
- [34] Laura Fumanelli, Marco Ajelli, Piero Manfredi, Alessandro Vespignani, and Stefano Merler. Inferring the structure of social contacts from demographic data in the analysis of infectious diseases spread. *PLoS Comput Biol*, 8(9):e1002673, 2012.
- [35] Sandro Galea, Raina M Merchant, and Nicole Lurie. The mental health consequences of covid-19 and physical distancing: the need for prevention and early intervention. *JAMA internal medicine*, 180(6):817–818, 2020.
- [36] Aurélien Gautreau, Alain Barrat, and Marc Barthélemy. Arrival time statistics in global disease spread. *Journal of Statistical Mechanics: Theory and Experiment*, 2007(09):L09001, 2007.
- [37] Aurélien Gautreau, Alain Barrat, and Marc Barthelemy. Global disease spread: statistics and estimation of arrival times. *Journal of theoretical biology*, 251(3):509–522, 2008.
- [38] Katy Gaythorpe and Ben Adams. Disease and disaster: optimal deployment of epidemic control facilities in a spatially heterogeneous population with changing behaviour. *Journal of theoretical biology*, 397:169–178, 2016.
- [39] Kathryn Glass and Belinda Barnes. Eliminating infectious diseases of livestock: a metapopulation model of infection control. *Theoretical population biology*, 85:63–72, 2013.

- [40] Jesús Gómez-Gardeñes, David Soriano-Panos, and Alex Arenas. Critical regimes driven by recurrent mobility patterns of reaction–diffusion processes in networks. *Nature Physics*, 14(4):391–395, 2018.
- [41] Bryan T Grenfell, Ottar N Bjørnstad, and Jens Kappey. Travelling waves and spatial hierarchies in measles epidemics. *Nature*, 414(6865):716–723, 2001.
- [42] Prince Harvim, Hong Zhang, Paul Georgescu, and Lai Zhang. Transmission dynamics and control mechanisms of vector-borne diseases with active and passive movements between urban and satellite cities. *Bulletin of mathematical biology*, 81(11):4518–4563, 2019.
- [43] Abigail L Horn and Hanno Friedrich. The network source location problem in the context of foodborne disease outbreaks. In *Dynamics on and of Complex Networks*, pages 151–165. Springer, 2017.
- [44] Abigail L Horn and Hanno Friedrich. Locating the source of large-scale outbreaks of foodborne disease. *Journal of the Royal Society Interface*, 16(151):20180624, 2019.
- [45] Zhao-Long Hu, Zhesi Shen, Shinan Cao, Boris Podobnik, Huijie Yang, Wen-Xu Wang, and Ying-Cheng Lai. Locating multiple diffusion sources in time varying networks from sparse observations. *Scientific reports*, 8(1):1–9, 2018.
- [46] Zhao-Long Hu, Zhesi Shen, Chang-Bing Tang, Bin-Bin Xie, and Jian-Feng Lu. Localization of diffusion sources in complex networks with sparse observations. *Physics Letters A*, 382(14):931–937, 2018.
- [47] ZL Hu, L Wang, and CB Tang. Locating the source node of diffusion process in cyber-physical networks via minimum observers. *Chaos: An Interdisciplinary Journal of Nonlinear Science*, 29(6):063117, 2019.
- [48] Damir Huremović. Brief history of pandemics (pandemics throughout history). In *Psychiatry of pandemics*, pages 7–35. Springer, 2019.
- [49] Flavio Iannelli, Andreas Koher, Dirk Brockmann, Philipp Hövel, and Igor M Sokolov. Effective distances for epidemics spreading on complex networks. *Physical Review E*, 95(1):012313, 2017.
- [50] Feng Ji, Wee Peng Tay, and Lav R Varshney. An algorithmic framework for estimating rumor sources with different start times. *IEEE Transactions on Signal Processing*, 65(10):2517–2530, 2017.
- [51] Jiaojiao Jiang, Sheng Wen, Shui Yu, Yang Xiang, and Wanlei Zhou. Rumor source identification in social networks with time-varying topology. *IEEE Transactions on Dependable and Secure Computing*, 15(1):166–179, 2016.
- [52] Yuhao Kang, Song Gao, Yunlei Liang, Mingxiao Li, and Jake Kruse. Multiscale dynamic human mobility flow dataset in the u.s. during the covid-19 epidemic. *Scientific Data*, pages 1–13, 2020.
- [53] Jung Eun Kim, Hyojung Lee, Chang Hyeong Lee, and Sunmi Lee. Assessment of optimal strategies in a two-patch dengue transmission model with seasonality. *PloS one*, 12(3):e0173673, 2017.
- [54] Glenn Lawyer. Measuring the potential of individual airports for pandemic spread over the world airline network. *BMC infectious diseases*, 16(1):1–10, 2015.
- [55] Sunmi Lee and Carlos Castillo-Chavez. The role of residence times in two-patch dengue transmission dynamics and optimal strategies. *Journal of theoretical biology*, 374:152–164, 2015.
- [56] Xiang Li, Xiaojie Wang, Chengli Zhao, Xue Zhang, and Dongyun Yi. Locating the epidemic source in complex networks with sparse observers. *Applied Sciences*, 9(18):3644, 2019.
- [57] Pedro G Lind, Luciano R Da Silva, José S Andrade Jr, and Hans J Herrmann. Spreading gossip in social networks. *Physical Review E*, 76(3):036117, 2007.
- [58] Yang Liu, Rosalind M Eggo, and Adam J Kucharski. Secondary attack rate and superspreading events for sars-cov-2. *The Lancet*, 395(10227):e47, 2020.
- [59] Andrey Y Lokhov, Marc Mézard, Hiroki Ohta, and Lenka Zdeborová. Inferring the origin of an epidemic with a dynamic message-passing algorithm. *Physical Review E*, 90(1):012801, 2014.
- [60] Alireza Louni and KP Subbalakshmi. A two-stage algorithm to estimate the source of information diffusion in social media networks. In *2014 IEEE Conference on Computer Communications Workshops (INFOCOM WKSHPs)*, pages 329–333. IEEE, 2014.

- [61] Nita Madhav, Ben Oppenheim, Mark Gallivan, Prime Mulembakani, Edward Rubin, and Nathan Wolfe. Pandemics: risks, impacts, and mitigation. *Disease control priorities: improving health and reducing poverty. 3rd edition*, 2017.
- [62] L Matthews, DT Haydon, DJ Shaw, ME Chase-Topping, MJ Keeling, and MEJ Woolhouse. Neighbourhood control policies and the spread of infectious diseases. *Proceedings of the Royal Society of London. Series B: Biological Sciences*, 270(1525):1659–1666, 2003.
- [63] Dror Meidan, Nava Schulmann, Reuven Cohen, Simcha Haber, Eyal Yaniv, Ronit Sarid, and Baruch Barzel. Alternating quarantine for sustainable epidemic mitigation. *Nature communications*, 12(1):1–12, 2021.
- [64] Stefano Merler and Marco Ajelli. The role of population heterogeneity and human mobility in the spread of pandemic influenza. *Proceedings of the Royal Society B: Biological Sciences*, 277(1681):557–565, 2010.
- [65] Denis Mollison. Spatial contact models for ecological and epidemic spread. *Journal of the Royal Statistical Society: Series B (Methodological)*, 39(3):283–313, 1977.
- [66] Denis Mollison, Kari Kuulasmaa, et al. Spatial epidemic models: theory and simulations. *Population dynamics of rabies in wildlife*, 8:291–309, 1985.
- [67] William Msemburi, Ariel Karlinsky, Victoria Knutson, Serge Aleshin-Guendel, Somnath Chatterji, and Jon Wakefield. The who estimates of excess mortality associated with the covid-19 pandemic. *Nature*, 613(7942):130–137, 2023.
- [68] World Health Organization et al. *The global burden of disease: 2004 update*. World Health Organization, 2008.
- [69] Robert Paluch, Xiaoyan Lu, Krzysztof Suchecki, Bolesław K Szymański, and Janusz A Hołyst. Fast and accurate detection of spread source in large complex networks. *Scientific reports*, 8(1):1–10, 2018.
- [70] Romualdo Pastor-Satorras, Claudio Castellano, Piet Van Mieghem, and Alessandro Vespignani. Epidemic processes in complex networks. *Reviews of modern physics*, 87(3):925, 2015.
- [71] Betty Pfefferbaum and Carol S North. Mental health and the covid-19 pandemic. *New England Journal of Medicine*, 383(6):510–512, 2020.
- [72] B Aditya Prakash, Jilles Vreeken, and Christos Faloutsos. Efficiently spotting the starting points of an epidemic in a large graph. *Knowledge and information systems*, 38(1):35–59, 2014.
- [73] Linda Rass, MA Lifshits, and John Radcliffe. *Spatial deterministic epidemics*. American Mathematical Soc., 2003.
- [74] Duncan A Robertson. Spatial transmission models: A taxonomy and framework. *Risk Analysis*, 39(1):225–243, 2019.
- [75] Tim Schlaich, Abigail L Horn, Marcel Fuhrmann, and Hanno Friedrich. A gravity-based food flow model to identify the source of foodborne disease outbreaks. *International journal of environmental research and public health*, 17(2):444, 2020.
- [76] Eunsoo Seo, Prasant Mohapatra, and Tarek Abdelzaher. Identifying rumors and their sources in social networks. In *Ground/air multisensor interoperability, integration, and networking for persistent ISR III*, volume 8389, page 83891I. International Society for Optics and Photonics, 2012.
- [77] Devavrat Shah and Tauhid Zaman. Rumors in a network: Who’s the culprit? *IEEE Transactions on information theory*, 57(8):5163–5181, 2011.
- [78] Sushila Shelke and Vahida Attar. Source detection of rumor in social network—a review. *Online Social Networks and Media*, 9:30–42, 2019.
- [79] Zhesi Shen, Shinan Cao, Wen-Xu Wang, Zengru Di, and H Eugene Stanley. Locating the source of diffusion in complex networks by time-reversal backward spreading. *Physical Review E*, 93(3):032301, 2016.
- [80] Dalila Talevi, Valentina Socci, Margherita Carai, Giulia Carnaghi, Serena Faleri, Edoardo Trebbi, Arianna di Bernardo, Francesco Capelli, and Francesca Pacitti. Mental health outcomes of the covid-19 pandemic. *Rivista di psichiatria*, 55(3):137–144, 2020.
- [81] Wenchang Tang, Feng Ji, and Wee Peng Tay. Estimating infection sources in networks using partial timestamps. *IEEE Transactions on Information Forensics and Security*, 13(12):3035–3049, 2018.

- [82] Alessandro Vespignani. Multiscale mobility networks and the large scale spreading of infectious diseases. In *APS March Meeting Abstracts*, volume 2010, pages A4–002, 2010.
- [83] Cécile Viboud, Ottar N Bjørnstad, David L Smith, Lone Simonsen, Mark A Miller, and Bryan T Grenfell. Synchrony, waves, and spatial hierarchies in the spread of influenza. *science*, 312(5772):447–451, 2006.
- [84] Haidong Wang, Katherine R Paulson, Spencer A Pease, Stefanie Watson, Haley Comfort, Peng Zheng, Aleksandr Y Aravkin, Catherine Bisignano, Ryan M Barber, Tahiya Alam, et al. Estimating excess mortality due to the covid-19 pandemic: a systematic analysis of covid-19-related mortality, 2020–21. *The Lancet*, 399(10334):1513–1536, 2022.
- [85] Hong-Jue Wang and Kai-Jia Sun. Locating source of heterogeneous propagation model by universal algorithm. *EPL (Europhysics Letters)*, 131(4):48001, 2020.
- [86] Zhaoxu Wang, Wenxiang Dong, Wenyi Zhang, and Chee Wei Tan. Rumor source detection with multiple observations: Fundamental limits and algorithms. *ACM SIGMETRICS Performance Evaluation Review*, 42(1):1–13, 2014.
- [87] Fan Wu, Su Zhao, Bin Yu, Yan-Mei Chen, Wen Wang, Zhi-Gang Song, Yi Hu, Zhao-Wu Tao, Jun-Hua Tian, Yuan-Yuan Pei, et al. A new coronavirus associated with human respiratory disease in china. *Nature*, 579(7798):265–269, 2020.
- [88] Lu Zhong, Mamadou Diagne, Weiping Wang, and Jianxi Gao. Country distancing reveals the effectiveness of travel restrictions during covid-19. *medRxiv*, 2020.

6 General Mathematical Framework

6.1 Notation of variables and parameters

Parameter	Name	Unit	Definition
β	Transmission rate	$\frac{1}{day}$	Transmission rate in the SIR dynamics
γ	Recovery rate	$\frac{1}{day}$	Recovery rate in the SIR dynamics
R_0	Basic reproduction rate	-	The transition rate over the recovery rate
q_i	-	-	the slope of the linear part of the dynamics for node i , see sections 6.4 and 6.5.
S_i	Susceptible in the sub-population i	-	Number of susceptible individuals in node i
I_i	Infected people in node i	-	Number of infected/infectious individuals in node i
I_i^e	Reported infected individuals in node i	-	Number of infected/infectious individuals in node i reported by (empirical data)
Δ_i	MSE	-	Mean squared error between I_i and I_i^e
i_0	Total initial patients	-	The total number of patients at the beginning of the dynamic (sum over $\vec{I}(0)$).
R_i	Recovered people in a sub-population i	-	Number of recovered individuals in node i
N	Total population	-	The total population studied within the meta-population
N_i	Population of the sub-population i	-	-
n	Number of sub-populations	-	-
N_p	Total passengers population	-	Number of daily travelers
F_{ij}	Flow per unit time	$\frac{1}{day}$	Number of daily travelers from the node i to the node j
P_{ij}	Passenger probability per unit time	-	Probability that a traveler travels from the node i to the node j
p	$\frac{N_p}{N}$	$\frac{1}{day}$	Travel probability of an individual between sub-populations
\hat{B}	Time evolving operator	-	See the main text
D_{ij}	Effective distance between node i and j	-	see Eq. 16
t_o^j	Overtaking time of node j	-	When the intra-population dynamics surpass the inter-population dynamics at node j , see Eq. 14

Table 1: All used parameters in our mathematical framework are brought here.

6.2 Definition of flow matrix and mobility probability Matrix

P_{ij} , is defined as the probability that a person travels from node i to node j . Also, p is defined as the average travel probability in the network. The *Flow Matrix* is a matrix representing the movements within the network. F_{ij} is the number of travellers from node i to j per time. So, $\sum_j F_{ij}$ is the total number of passengers exiting from the node i . Based on this definition, we make the probability matrix and the parameter p as the following:

$$P_{ij} = \frac{F_{ij}}{\sum_j F_{ij}} \quad (18)$$

$$p = \frac{\sum_j \sum_i F_{ij}}{N}, \quad (19)$$

where N is the total population of the network.

6.3 Deriving the intra population term in Eq. 3

To derive the number of infected people in node i , we have to calculate the flow of infected people in and out of this node. To calculate the number of infected people per time, who leave this node and go to other nodes, first, we can use the concept of flow and calculate the number of infected people that go to node j :

$$F_{ij} \frac{I_i}{N_i} \quad (20)$$

Then, we can sum over the index j to calculate the total number of people who leave the node i :

$$\sum_j F_{ij} \frac{I_i}{N_i}. \quad (21)$$

If we consider the travel probability in node i to be

$$p_i = \frac{\sum_j F_{ij}}{N_i}, \quad (22)$$

then we can rewrite the above equation and derive the following differential equation for the outgoing population in node i :

$$\frac{dI_i}{dt} = -p_i I_i \quad (23)$$

Now to calculate the number of infected people that enter node i , we calculate the number of infected people who travel from node j to i per time :

$$F_{ji} \frac{I_j}{N_j} \quad (24)$$

Then, if we multiply both the numerator and denominator by

$$\sum_i F_{ji} \quad (25)$$

the resulting equation is

$$\frac{F_{ji}}{\sum_i F_{ji}} \frac{\sum_i F_{ji}}{N_j} I_j. \quad (26)$$

The first term on the left side is the definition of a probability matrix, P_{ji} . So the number of infected people who travel from node j to i is

$$p_j P_{ji} I_j. \quad (27)$$

By summing up the above equation over index j , we have

$$\sum_j p_j P_{ji} I_j. \quad (28)$$

Now, the full evolution of infected people in node i is

$$\frac{dI_i}{dt} = -p_i I_i + \sum_j p_j P_{ji} I_j. \quad (29)$$

To derive the final formula, we assume the travel probability is the same among the nodes of the network and is equal to the average value of being a traveler in the whole network. Therefore

$$p_i \approx p = \frac{\sum_j \sum_i F_{ij}}{N}, \quad (30)$$

which means

$$\frac{dI_i}{dt} = -pI_i + p \sum_j P_{ji} I_j. \quad (31)$$

6.4 Deriving exponential behavior of $\vec{I}(t)$ in the early stage of the dynamic (Eq. 2)

Assuming the spread of the disease is at its early stages, we can estimate S_i with N_i and rewrite the evolution equation as

$$S_i \approx N_i \quad (32)$$

$$\frac{dI_i}{dt} = (\beta_i N_i - \gamma_i - p) I_i + \sum_j p P_{ji} I_j, \quad (33)$$

in which P_{ij}^T and q_i as,

$$P_{ij}^T = P_{ji} \quad (34)$$

$$q_i = \frac{\beta_i N_i - \gamma_i}{p}. \quad (35)$$

The equation can be rewritten as

$$\frac{dI_i}{dt} = p \sum_j (P_{ij}^T + \delta_{ij}(q_j - 1)) I_j, \quad (36)$$

where δ_{ij} is the Kronecker delta and is equal to 1 when $i = j$ and zero when $i \neq j$. Considering $B_{ij} = P_{ij}^T + \delta_{ij}(q_j - 1)$, the above equation can be simplified as

$$\frac{d\vec{I}}{dt} = p \hat{B} \vec{I}, \quad (37)$$

in which matrix \hat{B} is

$$\hat{B} = \begin{bmatrix} q_1 - 1 & P_{21} & P_{31} & \dots \\ P_{12} & q_2 - 1 & P_{32} & \dots \\ \dots & \dots & \dots & \dots \end{bmatrix} \quad (38)$$

The solution to the above differential vector equation is

$$\vec{I}(t) = e^{\hat{B}pt} \vec{I}(0), \quad (39)$$

where, $\vec{I}(0)$ represents the initial vector of patients.

6.5 Deriving q_i in the early stage of dynamics

Assuming the spread of the disease is at early stages in the SIR model, we can estimate S_i with N_i and rewrite the evolution equation as

$$S_i \approx N_i \quad (40)$$

$$\frac{dI_i}{dt} = \beta_i N_i I_i - \gamma_i I_i, \quad (41)$$

with the solution of

$$I_i(t) = I_i(0) e^{\frac{\beta_i N_i - \gamma_i}{p}(pt)}. \quad (42)$$

The above equation can be rewritten in the simpler form of

$$I_i(t) = I_i(0) e^{q_i(pt)}. \quad (43)$$

As a result, we can expect a linear behavior if we plot $\log I_i(t)$ vs pt

$$\log I_i(t) = \log I_i(0) + q_i(pt). \quad (44)$$

The slope of this line is q_i .

6.6 $e^{\hat{B}pt}$ expansion and intermediary nodes

Eq. 39 can be expanded as

$$\vec{I}(t) = (\hat{1} + \hat{B}pt + \frac{(\hat{B}pt)^2}{2!} + \dots)\vec{I}(0), \quad (45)$$

where $\hat{1}$ is the identity matrix. If we label the source node with i , and the non-source nodes with j , for node j the above equation leads to :

$$P_{ij}i_0pt + \left[\frac{i_0p^2t^2}{2} ((P_{ij})(q_i + q_j - 2) + P_{i1}P_{1j} + P_{i2}P_{2j} + \dots + P_{in}P_{nj}) + \dots \right] \quad (46)$$

In the above equation, the term :

$$P_{i1}P_{1j} + P_{i2}P_{2j} + \dots P_{in}P_{nj} = \sum_k P_{ik}P_{kj}$$

is the probability that one travels from node i to j via one of the intermediary nodes between them. We name it P_{ij}^1 , therefore:

$$I_j(t) = P_{ij}i_0pt + \frac{i_0p^2t^2}{2} (P_{ij}(q_i + q_j - 2) + P_{ij}^1) + \dots \quad (47)$$

For the source node, the evolution equation is

$$I_i(t) = i_0(1 + pt(q_i - 1)) + \dots \quad (48)$$

7 Algorithms and Results

7.1 Details of Where algorithm

Assume one has a snapshot of the disease state reported exactly t days after the beginning of the pandemic:

$$(I_1^e, I_2^e, \dots, I_n^e). \quad (49)$$

The goal is to find the sources given the starting time and a snapshot of the disease.

We know that the dynamic of $\vec{I}(t)$ is:

$$\vec{I}(t) = e^{\hat{B}pt}\vec{I}(0) \quad (50)$$

If there are some nodes responsible for the spread of the disease in the network with the initial number of patient of $i_{0_i}, i_{0_j}, i_{0_k}, \dots$, then $\vec{I}(0)$ can be decomposed into a summation of different initial vectors, each representing a specific node. Therefore we have

$$\vec{I}(t) = e^{\hat{B}pt}(\vec{I}_i(0) + \vec{I}_j(0) + \vec{I}_k(0) + \dots) \quad (51)$$

$$\vec{I}(t) = \vec{I}_i(t) + \vec{I}_j(t) + \dots, \quad (52)$$

where

$$\vec{I}_i(t) = e^{\hat{B}pt}\vec{I}_i(0). \quad (53)$$

Now if we define the basis vector \vec{i} to be a vector with 1 in component i and 0 in all other components, we can write:

$$\vec{I}_i(0) = i_{0_i}\vec{i} \quad (54)$$

$$\vec{I}(t) = (e^{\hat{B}pt}i_{0_i}\vec{i} + e^{\hat{B}pt}i_{0_j}\vec{j} + \dots). \quad (55)$$

So if we change our basis from \vec{i} into \vec{i}' :

$$\vec{i}' = e^{\hat{B}pt}\vec{i}, \quad (56)$$

it can be easily shown that in the linear range, these new bases are complete and orthogonal. Now, we define the "weight of a node" as

$$W_i = \frac{\vec{i}' \cdot \vec{I}(t)}{\sum_{\vec{i}'} \vec{i}' \cdot \vec{I}(t)}. \quad (57)$$

W_i is a number between 0 and 1 and shows the contribution of the node i at the beginning of the spread. If W_i is 1 it means that node i was responsible alone. So by calculating the defined weight for different nodes, we can understand the role and impact of each node on the spread.

7.2 Details of When algorithm

Assuming to have a snapshot of the state of the disease at a specific time written down as a vector:

$$\vec{I}^e = (I_1^e, I_2^e, \dots, I_n^e) \quad (58)$$

where I_i^e represents the number of infected people in its corresponding node. n is the number of nodes in the network. We aim to determine the starting time of the disease using both the model and the snapshot. We define MSE (Mean Squared Error) as a closeness parameter for two vectors:

$$\Delta_i(t) = \frac{\sum_{j=1}^n (I_j - I_j^e)^2}{n} \quad (59)$$

in which i is the index of the source and I_j is the number of patients in the node j predicted by the model.

Now, we calculate the closeness parameter of the snapshot vector and the disease vector that comes out of the theory (using the first and the second term) in a determined time t :

$$\Delta_i^{\kappa=1}(t) = \frac{1}{n}((i_0(1 + (\beta N_i - \gamma - p)t) - I_i^e)^2 + \sum_{i=j, j \neq i}^n (P_{ij} p t i_0 - I_j^e)^2) \quad (60)$$

To find the minimum of the closeness parameter, we calculate the derivative of the above equation with respect to the t ($\frac{d\Delta_m(t)}{dt} = 0$)

$$t_i^* = \frac{1 - \eta(i_0 - I_i^e) + p \sum (P_{ij} I_j^e)}{i_0 \eta^2 + p^2 \sum P_{ij}^2} \quad (61)$$

in which $\eta = (\beta N_m - \gamma - p)$.

It means that the theory predicts the snapshot belongs to t days after the start of the disease. So the overtaking time would be t days before the date of the snapshot.

7.3 Error in When algorithm

In this subsection we want to explain the way we estimated the error in When algorithm. It is crucial to note that the source of error in this algorithm is coming from the additional term in the Taylor expansion. In this case, for the source node, the dynamic is:

$$I_i(t) = C + A_i t + B_i t^2 \quad (62)$$

And for non-source nodes, the dynamic is :

$$I_j(t) = A_j t + B_j t^2 \quad (63)$$

The A,B,C coefficients are constants that are calculated via Eq.47 and Eq.48. Now we define MSE parameter:

$$\Delta = (C + A_i t + B_i t^2 - I_i^e)^2 + \sum_j (A_j t + B_j t^2 - I_j^e)^2 \quad (64)$$

which leads to the following equation:

$$\Delta = \Delta_0 + 2t^2((C - I_i^e)B_i - \sum_j (I_j^e B_j)t^2) \quad (65)$$

By rewriting the right term in the above equation:

$$\eta = 2(C - I_i^e)B_i - \sum_j (I_j^e B_j) \quad (66)$$

We are able to rewrite the MSE parameter :

$$\Delta = \Delta_0 + \eta t^2 \quad (67)$$

Now, by applying the derivative condition to the new equation :

$$\frac{d\Delta}{dt} = \frac{d\Delta_0}{dt} + 2\eta t = 0 \quad (68)$$

The condition of having zero value derivative happens in:

$$\frac{d\Delta_0}{dt} = -2\eta t \quad (69)$$

To find the specific point that the above condition is met, we use the Taylor expansion of Δ_0 function in the minimum point of the function(t^*).

$$\Delta_0(t) = \Delta_0(t^*) + \frac{1}{2} \frac{d^2\Delta_0(t)}{dt^2} (\delta t)^2 + \dots \quad (70)$$

In the above equation, the first derivative term is equal to zero since the Δ_0 function is in its minimum in t^* . Then by substituting the Taylor expansion, we have :

$$\frac{\delta t}{t} = \frac{\eta}{\frac{d^2\Delta_0}{dt^2}} \quad (71)$$

7.4 Details of Effective Distance algorithm

In this part, we define the overtaking time of a disease in a specific node as the time when intra-population dynamics surpass the inter-population dynamic. The critical mathematical condition for this state for node j is :

$$(N_j\beta_j - \gamma_j)I_j = p\left(\sum_k P_{kj}I_k - I_j\right) \quad (72)$$

If we rewrite this equation, we have:

$$p\left(\sum_k P_{kj}I_k\right) - (\beta_j - \gamma_j + p)I_j = 0 \quad (73)$$

So if we define vector \vec{A}_j for the j -th node:

$$\vec{A}_j = (P_{1j}, P_{2j}, \dots, -(q_j + 1), \dots, P_{nj}) \quad (74)$$

In which $-(q_j + 1)$ is in the j th component.

Now, we can write the critical condition for node j in a simpler way:

$$\vec{A}_j \cdot \vec{I} = 0 \quad (75)$$

If we want to calculate the overtaking time for node j , we can use the evolution equation of \vec{I} :

$$\vec{I}(t) = \vec{I}(0) + pt\hat{B}\vec{I}_0 \quad (76)$$

If we dot product the vector \vec{A}_j in both sides of the above equation and set the left side of the equation to be zero :

$$0 = \vec{A}_j \cdot \vec{I}_0 + pt_A \vec{A}_j \cdot \hat{B}\vec{I}_0 \quad (77)$$

So the overtaking time would be:

$$t_O^j = -\frac{1}{p} \frac{\vec{A}_j \cdot \vec{I}_0}{\vec{A}_j \cdot \hat{B}\vec{I}_0}$$

If we assume the i th Node to be the source, the \vec{I}_0 would be :

$$\vec{I}_0 = i_0(0, 0, \dots, 1, \dots, 0)$$

In which the 1 is in the i th component. Therefore, the numerator of the overtaking time equation would be: $P_{ij}I_0$

For calculating the denominator, first we have to calculate $\hat{B}\vec{I}_0$ that would be :

$$\hat{B}\vec{I}_0 = i_0(P_{i1}, P_{i2}, \dots, q_i - 1, \dots, P_{in}) \quad (78)$$

In which the $q_i - 1$ term is in the i th component. Now we have to calculate the $\vec{A}_j \cdot \hat{B}\vec{I}_0$ that would be:

$$i_0(P_{ij}^1 - (2 + q_j - q_i)P_{ij}) \quad (79)$$

In which $P_{ij}^1 = \sum_k P_{ik}P_{kj}$

So by substituting these terms in the overtaking time equation, we have :

$$t_O^j = \frac{1}{p} \frac{1}{(2 + q_j - q_i) - \frac{P_{ij}^1}{P_{ij}}} \quad (80)$$

7.5 Error in Effective Distance algorithm

In this subsection, we aim to explain the way we estimated error in Effective Distance algorithm. The source of error here, is the additional term in the Taylor expansion. So if we keep the second term of the expansion, we have :

$$I(\vec{t}) = I_0(\vec{t}) + pt\hat{B}\vec{I}_0 + \frac{1}{2}(pt)^2\hat{B}^2\vec{I}_0 \quad (81)$$

Now by applying the condition of overtaking in node j :

$$0 = \vec{A}_j \cdot \vec{I}_0 + pt_j(\vec{A}_j \hat{B} \vec{I}_0) + \frac{1}{2}(pt_j)^2(\vec{A}_j \cdot \hat{B}^2 \vec{I}_0) \quad (82)$$

By rewriting time we have:

$$t_j = t_j^* + \delta t_j \quad (83)$$

In which, t_j^* is the overtaking time when we only consider the first term of the expansion. hence the equation will be in this form:

$$0 = \vec{A}_j \cdot \vec{I}_0 + pt_j^* \vec{A}_j \hat{B} \vec{I}_0 + p\delta t_j \vec{A}_j \hat{B} \vec{I}_0 + \frac{1}{2}(p(t_j^* + \delta t))^2 \vec{A}_j \hat{B}^2 \vec{I}_0 \quad (84)$$

The first two terms in the right-hand side of the equation will cancel each other out. By simplification of the above equation the final equation for the error will be :

$$\frac{\delta t_j}{t_j^*} = \frac{-pt_j^* \vec{A}_j \cdot \hat{B}^2 \vec{I}_0}{2(pt_j^* \vec{A}_j \cdot \hat{B}^2 \vec{I}_0 + \vec{A}_j \cdot \hat{B} \vec{I}_0)} \quad (85)$$

7.6 How to estimate Effective Distance without mobility data

In the previous subsection we introduced a new definition of effective distance and showed its linear relation with the overtaking time. There are two challenges when it comes to the approval of the relations with empirical data. First, The exact value of overtaking time is not known. Second, the exact value of the probability matrix is not accessible, especially after the quarantine policy in each country. In this section, we aim to bring up a novel data analysis method to overcome these challenges and confirm our theoretical achievements with empirical data. We have shown in previous sections that the temporal evolution of infected numbers is known for each node based on the general theory. Also, we know that the most accurate and accessible empirical data is the number of infected people in each node. So If we could rewrite our definition of effective distance in a way that only the number of infected people would be needed, we can achieve a new way to check our claims. Also, using official daily number of patients in different cases, we've estimated each node's overtaking time. We will show that there is a high correlation between effective distance and the estimated overtaking times.

Consider the number of infectious people versus time. Since the initial value is zero for non-source nodes, one can rewrite the equation for non-source nodes by rescaling time from t into $T = pt$:

$$I_j = A_j T + B_j T^2 \quad (86)$$

where I_j is the number of patients in the non-source node j , $A_j = P_{ij}i_0$, and $B_j = \frac{1}{2}(P_{ij}^1 + P_{ij}(q_i + q_j - 2))$. With a simple algebra on Eq. 80 the effective distance can be rewritten according to A_j and B_j as :

$$D_{ij} = \frac{1}{q_j - \frac{B_j}{A_j}} \quad (87)$$

It is worth noting that Eq. 87 is independent of i_0 , the initial number of patients, which is challenging to find at the beginning of a pandemic.

Now, we can calculate A_j and B_j by fitting a parabola to each non-source node patient data. However, there is a likely gap between official and empirical data owing to the fact that it takes several days for governments to identify patients at the beginning. Therefore, to fit, we've used

$$I_j = Q_j + A_j T + B_j T^2 \quad (88)$$

in which Q_j is the gap.

Moreover, to find q_j , it is enough to fit a line to the semi-log plot of patients- time, where it represents an acceptable exponential behavior, resulting from the SIR dynamics. The slop is equal to q_j .

The predicted overtaking time is the time when the number of patients is zero. After the coefficients were found, it can be calculated by solving the

$$0 = Q_j + A_j T + B_j T^2 \quad (89)$$

which leads to

$$T = \frac{-A_j + \sqrt{A_j^2 - 4Q_jB_j}}{2A_j}. \quad (90)$$

The differences in the regression of lines and number of points in this algorithm come from the accuracy of the raw data and also the mathematical condition ($\frac{P_{ij}^1}{P_{ij}} < 2$) that constrain the presence of some nodes in our calculation in different scenarios

It is worth noting that in our formalism the linear relation between Effective distance and overtaking time has y-intercept of zero and the source node has to be in (0,0) naturally. But in Figure.5 we observe that y-intercept has a non-zero value, which could be interpreted as a shift in the values of empirical overtaking times.

8 Using SEIR instead of SIR

If we consider the SEIR dynamic and its equations:

$$\frac{dE}{dt} = \beta IS - \sigma E \quad (91)$$

$$\frac{dI}{dt} = \sigma E - \gamma I \quad (92)$$

By substituting E from the first equation and putting it into the second, we will have :

$$\frac{dI}{dt} = \beta IS - \gamma I - \frac{dE}{dt} \quad (93)$$

In the first stages of the dynamic we can use two assumptions:

First, we can consider the S to be the total population which is N:

$$S = N \quad (94)$$

Also, we assume that the βI is small in comparison to the σE so the first equation would be in the form of :

$$\frac{dE}{dt} = -\sigma E \quad (95)$$

By using this equation we will have:

$$\frac{dI}{dt} = \beta IN - \gamma I + \sigma E(0) \quad (96)$$

Compared to the SIR model, now the solution of our model (by combining the effect of mobility) would be :

$$I(\vec{t}) = e^{\hat{B}pt} I(\vec{0}) + \sigma E(\vec{0})t \quad (97)$$

If we expand this equation, we will have:

$$I(\vec{t}) = (\hat{I} + \hat{B}pt + \dots)I(\vec{0}) + \sigma E(\vec{0})t \quad (98)$$

We can summarize the above equation in this form :

$$I(\vec{t}) = I(\vec{0}) + (\hat{B}ptI(\vec{0}) + \sigma E(\vec{0})t) \quad (99)$$

Now by applying the Overtaking condition for node j :

$$I(\vec{t}) \cdot \vec{A}_j = 0 \quad (100)$$

we will have :

$$0 = I(\vec{0}) \cdot \vec{A}_j + (\hat{B}pI(\vec{0}) \cdot \vec{A}_j + \sigma E(\vec{0}) \cdot \vec{A}_j)t \quad (101)$$

So the overtaking time will be:

$$\frac{-I(\vec{0}) \cdot \vec{A}_j}{(\hat{B}I(\vec{0}) \cdot \vec{A}_j + \frac{\sigma}{p} E(\vec{0}) \cdot \vec{A}_j)} = pt_o \quad (102)$$

By using Taylor expansion :

$$\frac{-I(\vec{0}) \cdot \vec{A}_j}{(\hat{B}I(\vec{0}) \cdot \vec{A}_j + \frac{\sigma}{p} E(\vec{0}) \cdot \vec{A}_j)} = pt_o \quad (103)$$

9 Data

In this study, we primarily utilized two different types of data: A) Snapshots of active infected cases in each subpopulation during the linear phase, some of which are visualized in Fig. 2, panels *A* and *A'*, and B) Coarse-grained representations of inter-population mobility, illustrated in Fig. 2, panels *B* and *B'*. Both data types were used for Figs. 2 and 3, while only mobility data were used for Fig. 4, and only infected cases were used for Fig. 5, see section 7.6 for more details.

We obtained the number of infected people during the COVID-19 pandemic for different provinces of Iran from official reports by the Ministry of Health and Medical Education of Iran, which are available in Persian at request, and from The COVID Tracking Project at The Atlantic [31] for different states of the US. Data regarding the H1N1 pandemic was downloaded from "www.who.int". Abbreviations for Iranian provinces and American states are listed in Sec. 9.1.

The daily mobility data, which encompasses all forms of transportation for Iran (provided by the Basir company) and the USA [52], is averaged from March 1st to 3rd, 2020, for Iran, and from January to April 2020 for the USA.

9.1 Abbreviation

State	Abv.	State	Abv.	State	Abv.	State	Abv.
Alabama	AL	Alaska	AK	Arizona	AZ	Arkansas	AR
California	CA	Colorado	CO	Connecticut	CT	Delaware	DE
Columbia	DC	Florida	FL	Georgia	GA	Idaho	ID
Kentucky	KY	Louisiana	LA	Maine	ME	Maryland	MD
Illinois	IL	Indiana	IN	Iowa	IA	Kansas	KS
Kentucky	KY	Louisiana	LA	Maine	ME	Maryland	MD
Massachusetts	MA	Michigan	MI	Minnesota	MN	Mississippi	MS
Missouri	MO	Montana	MT	Nebraska	NE	Nevada	NV
NewHampshire	NH	New Jersey	NJ	New Mexico	NM	New York	NY
North Carolina	NC	North Dakota	ND	Ohio	OH	Oklahoma	OK
Oregon	OR	Pennsylvania	PA	Rhode Island	RI	South Carolina	SC
South Dakota	SD	Tennessee	TN	Texas	TX	Utah	UT
Vermont	VT	Virginia	VA	Washington	WA	West Virginia	WV
Wisconsin	WI	Wyoming	WY	–	–	–	–

Table 2: Abbreviation of the US states.

Province	Abv.	Province	Abv.
Ardabil	AR	Sistan-Baluchestan	SB
Ilam	IL	Golestan	GL
Khorasan-North	KS	Gilan	GI
Kurdistan-South	KJ	Yazd	YZ
Kermanshah	KM	Zanjan	ZN
Kordestan	KD	Kohgiluyeh-Boyer-Ahmad	KB
Bushehr	BU	ChaharMahaal-Bakhtiari	CB
Khorasan-Razavi	KR	Mazandaran	MZ
Khuzestan	KZ	Hormozgan	HR
Kerman	KN	Hamadan	HM
Lorestan	LR	Azerbaijan-West	AG
Qom	QM	Azerbaijan-East	AS
Semnan	SM	Fars	FR
Isfahan	ES	Qazvin	QZ
Markazi	MK	Alborz	AL
Tehran	TH		

Table 3: Abbreviation of provinces of Iran.

10 Sensitivity Analysis

These plots represent the sensitivity analysis in which γ has been changed from $\frac{1}{13}$ to $\frac{1}{20}$ and R_0 which is the basic reproductive number has been changed from 2.5 to 4.5. By using the day 5 from the official start of the pandemic we can say the 5 maximum provinces in the node power list is Qom, Tehran, Gilan, Markazi and Alborz. These provinces stay sorted in this format for all the values of R_0 and γ . As the R_0 increases the value of error increases too. As γ decreases the value of error decreases. But by looking at 10 days we can see that the place of Tehran and Qom has been swaped. Alborz came to the third place and got the previous position of Gilan. But pay attention that all these names remain reserved in the 10 days. But in 20 days Semnan appears in the list.

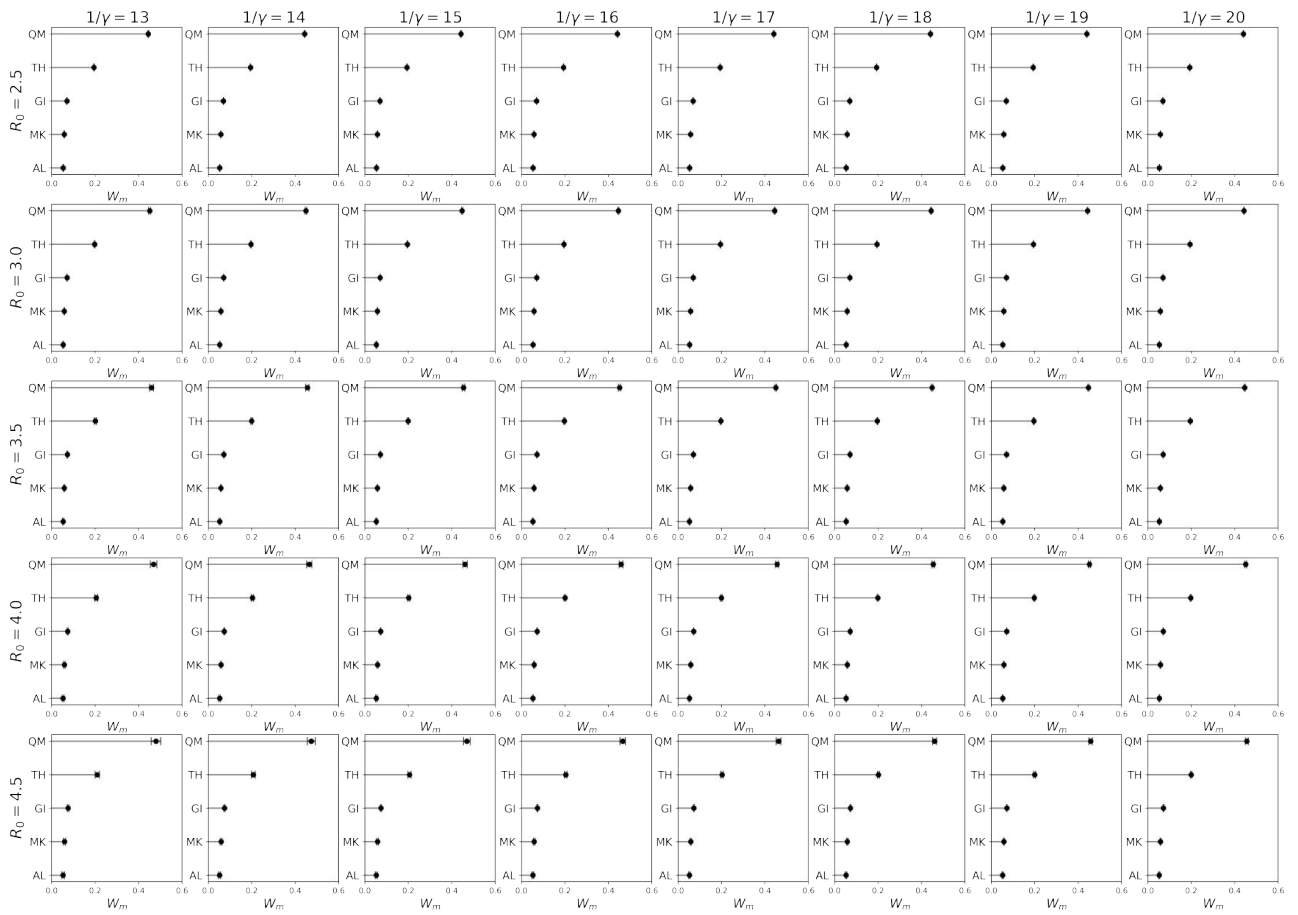


Figure 6: Calculated W_m for different provinces of Iran, and for different values of R_0 and γ , using the number of infected people in the fifth day of the COVID-19 pandemic in Iran.

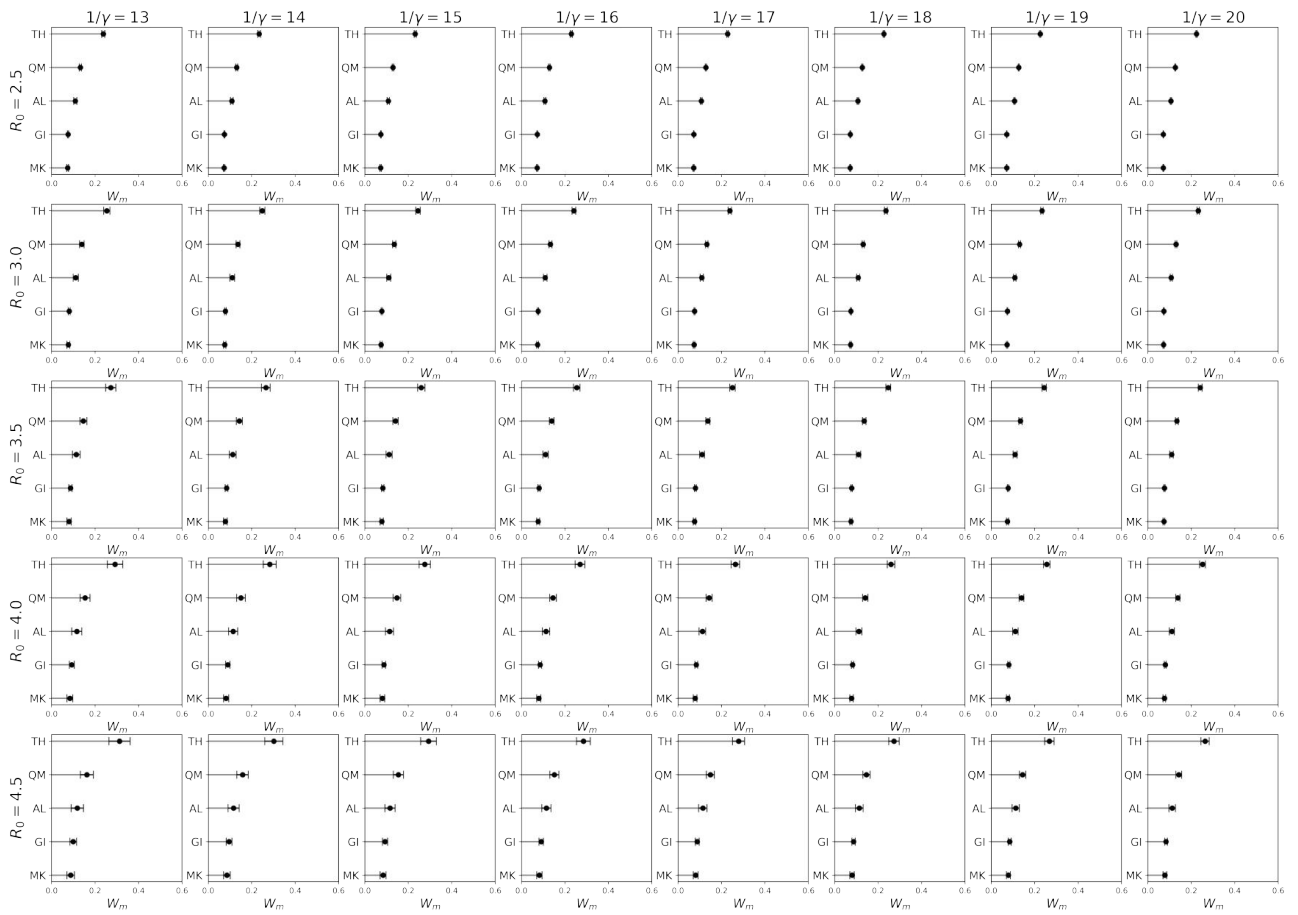


Figure 7: Calculated W_m for different provinces of Iran, and for different values of R_0 and γ , using the number of infected people in the tenth day of the COVID-19 pandemic in Iran.

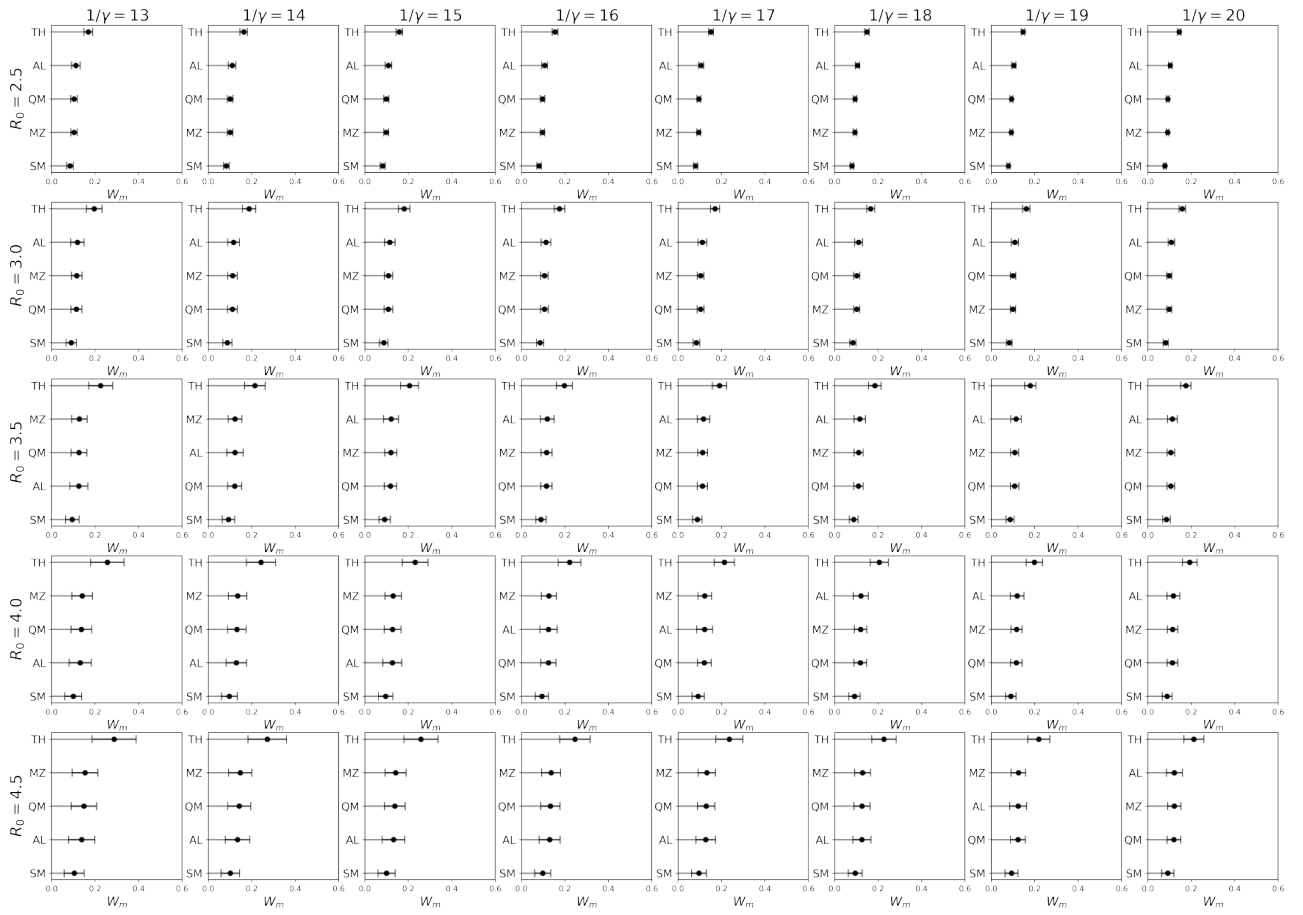


Figure 8: Calculated W_m for different provinces of Iran, and for different values of R_0 and γ , using the number of infected people in the fifteenth day of the COVID-19 pandemic in Iran.



Figure 10: Calculated W_m for different states of the US, and for different values of R_0 and γ , using the number of infected individuals in day 50 of the COVID-19 pandemic in the US.

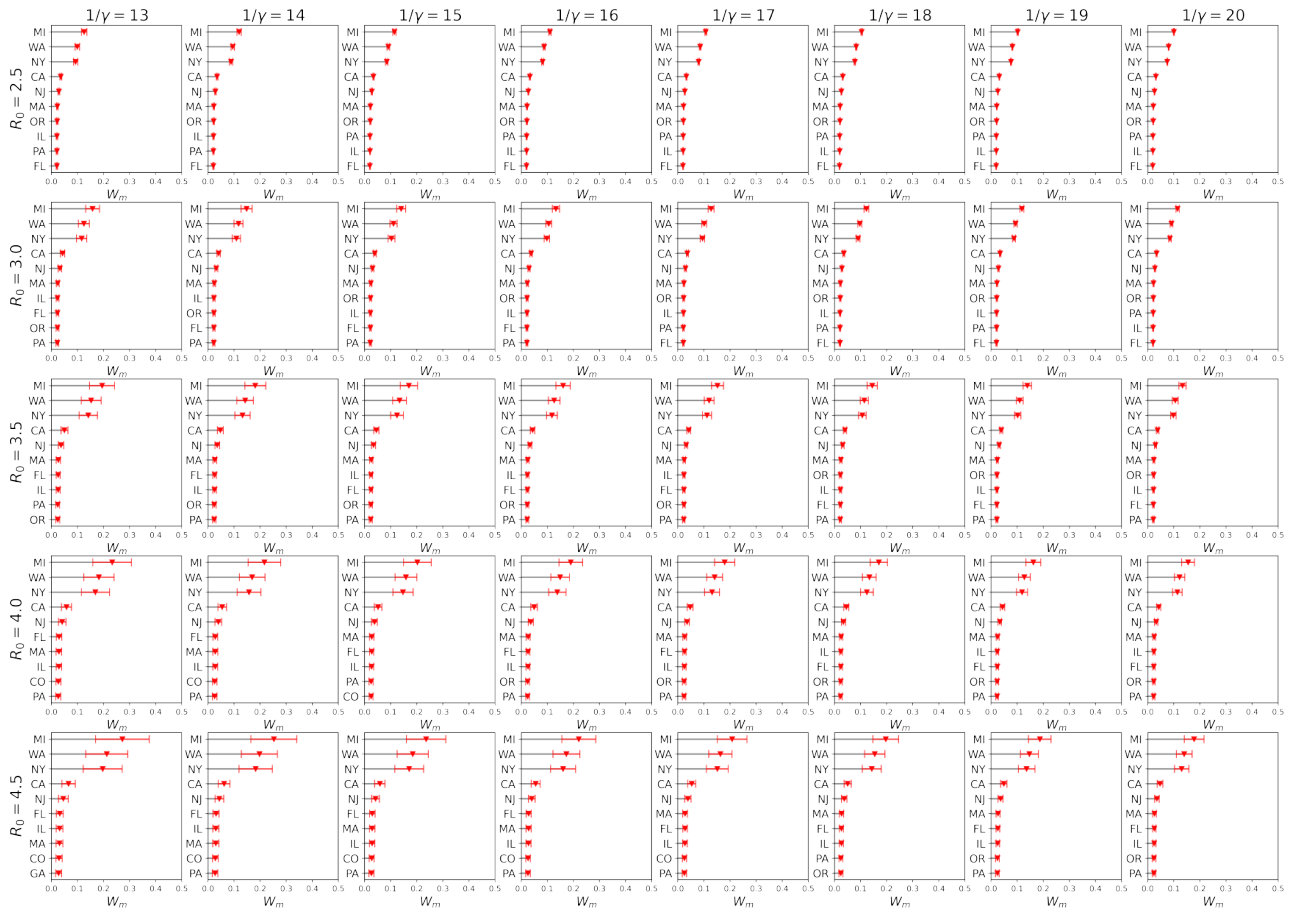


Figure 11: Calculated W_m for different states of the US, and for different values of R_0 and γ , using the number of infected individuals in day 55 of the COVID-19 pandemic in the US.